NASA Contractor Report 174831
UTRC Report R84-915540-34

Turbulent Transport and Length Scale Measurement Experiments with Confined Coaxial Jets

Bruce V. Johnson
Richard Roback

UNITED TECHNOLOGIES RESEARCH CENTER
East Hartford, CT 06108

CONTRACT NAS3-22771
November 1984

NASA
National Aeronautics and Space Administration

Lewis Research Center
Cleveland, Ohio 44135

NASA Contractor Report 174831
UTRC Report R84-915540-34

Turbulent Transport and Length Scale Measurement Experiments with Confined Coaxial Jets

TABLE OF CONTENTS

FOREWORD

This interim summary report covers the Phase III effort under contract NAS3-22771.

Following are the formal reports issued under Contract NAS3-22771:

1. Johnson, B. V. and J. C. Bennett: Mass and Momentum Turbulent Transport Experiments with Confined Coaxial Jets. NASA Contractor Report NASA CR-165574, November 1981 (Also issued as UTRC Report R81-915540-9).

2. Roback, R. and B. V. Johnson: Mass and Momentum Turbulent Transport Experiments with Confined Swirling Coaxial Jets. NASA Contractor Report NASA-CR-168252, August 1983 (Also issued as UTRC Report R83-915540-26).

3. Chiapetta, L. M.: Users Manual for a TEACH Computer Program for the Analysis of Turbulent, Swirling Reacting Flow in a Research Combustor. UTRC Report R83-915540-27, September 1983.

4. Johnson, B. V. and R. Roback: Turbulent Transport Experiments with Confined Nonswirling and Swirling Coaxial Jets. NASA Contractor Report NASA CR-174831, November 1984 (Also issued as UTRC Report R84-915540-34), (present report).

The following sound film supplements to Reports 1 and 2 have been produced by Dr. C. J. Marek and the NASA Lewis Audio-Visual Department:

5. NASA Lewis Research Center Sound Film Supplement C-303 to Report NASA-CR 165574.

6. NASA Lewis Research Center Sound Film Supplement C-311 to Report NASA-CR 168252.

The results obtained under Contract NAS3-22771 have been presented at the following NASA Lewis Research Center conferences:

7. Combustion Fundamentals Research Conference, October 21-22, 1982. NASA Conference Publication 2268, pp. 131-140.

8. Turbine Hot Section Technology 1983, October 25 and 26, 1983. NASA Conference Publication 2289, pp. 149-151.

9. Combustion Fundamentals Research Conference, April 16-18, 1984. NASA Conference Publication 2309, pp. 115-124.

10. Turbine Hot Section Technology 1984, October 23-24, 1984, pp. 189-198.

Data obtained under Contract NAS3-22771 has been included in the following presentations and publications:

11. Johnson, B. V. and J. C. Bennett: Statistical Characteristics of Velocity Concentrations Mass Transport and Momentum Transport for Coaxial Jet Mixing in a Confined Duct. Presented at 28th International Gas Turbine Conference, March 27-31, 1983. Published in ASME Journal of Enginering for Gas Turbine and Power, Vol. 106, pp. 121-127, January 1984.

12. Johnson, B. V. and J. C. Bennett: Mass and Momentum Turbulent Transport Experiments with Confined Coaxial Jets. Presented at Fourth Symposium on Turbulent Shear Flows, September 12-14, 1983. Published in Proceedings, pp. 1814-1819.

13. Johnson, B. V.: Turbulent Transport Experiment for Combustor Modeling: Presented at 1983 AFOSR Contractors Meeting on Air Breathing Combustor Dynamics Research, September 19-22, 1983.

14. Bennett, J. S. and B. V. Johnson: Turbulent Transport Measurements Using Laser Induced Fluoresence. Presented at the American Physical Society Fluid Dynamics Division Meeting, November 21-23, 1983.

15. Johnson, B. V.: Scalar and Momentum Turbulent Transport Experiments with Swirling Coaxial Jets, Presented at JANNAF Swirl Workshop, Reno NV, January 12, 1984.

16. Johnson, B. V. and R. Roback: Mass and Momenum Turbulent Transport Experiments with Confined Swirling Coaxial Jets. Presented at AIAA/SAE/ASME 20th Joint Propulsion Conference, June 11-13, 1984. Published as AIAA Preprint AIAA-84-1380.

17. Roback, R., B. V. Johnson and J. C. Bennett: Turbulent Transport Measurements Using a Combined Laser Velocimeter-Laser Induced Fluorescence Technique. Presented at Ninth Biennial Symposium on Turbulence, U. of Missouri-Rolla, October 1-3, 1984.

18. Johnson, B. V., R. Roback, J. C. Bennett: Scalar and Momentum Turbulent Transport Experiments with Swirling and Nonswirling Flows. Proceedings of Symposium on Experimental Measurements and Techniques in Turbulent Reactive and Nonreactive Flows, ASME, December 1984, p. 107-119.

ACKNOWLEDGEMENTS

The authors wish to acknowledge the participation of the following persons in the development of the computerized length scale measurement technique used to obtain data presented in this report: Dr. J. C. Bennett (University of Connecticut), Mr. W. Daniels and Ms. S. Orr. The development of the computerized length scale measurement technique was jointly supported by the Pratt & Whitney Engineering Division (Combustion Group) and the United Technologies Research Center under their independent research programs.

SUMMARY

A three phase experimental study of mixing downstream of swirling and nonswirling confined coaxial jets has been conducted to obtain data for the evaluation and improvement of turbulent transport models currently employed in a variety of computational procedures used throughout the propulsion community. The present effort (Phase III) effort was directed toward (1) the acquisition of length scale and dissipation rate data that provide more accurate inlet boundary conditions for the computational procedures and a data base to evaluate the turbulent transport models in the near jet region where recirculation does not occur, and (2) the acquisition of mass and momentum turbulent transport data for a nonswirling flow condition with a blunt inner-jet inlet configuration rather than the tapered inner-jet inlet employed in Phase I. The total study has been comprised of mass and momentum turbulent transport experiments, flow visualization studies, the documentation and checkout of a computer program, and the measurement of dissipation rate and integral length scales. A nonswirling coaxial jet study was conducted and reported under Phase I using a tapered wall inner jet inlet configuration. A swirling coaxial flow study, using the same inner jet configuration, was conducted and reported under Phase II. A TEACH code was also acquired, checked out for several cases, and reported under Phase II of the contract.

The measurement technique, generally used to obtain approximate integral length and microscales of turbulence and dissipation rates, was recently computerized at UTRC. This computerized data acquisiton and reduction procedure was used to obtain length scale and dissipation rate data for three test configurations. The most extensive set of data was obtained with the tapered inner jet inlet configuration for the nonswirling flow condition. Results showed the dissipation rate varied by 2 1/2 orders of magnitude at the inlet plane, by 2 orders of magnitude 51 mm (2 in.) from the inlet plane, and by 1 order of magnitude at 102 mm (4 in.) from the inlet plane. The ratio of the integral scale length for the streamwise velocity component to the microscale length varied from values of 2 to 6 between the inlet plane and the 102 mm location.

Mass and momentum turbulent transport data was obtained downstream of the blunt inner-jet inlet configuration, using the laser velocimeter/laser induced fluorescence measurement techniques employed in the previous experiments with swirling and nonswirling flow conditions. The velocities, concentrations and momentum turbulent transport results obtained downstream of the blunt inner-jet inlet configuration for the nonswirling flow condition were not significantly different from those obtained with the tapered inner-jet inlet. The results are presented and compared with the Phase I results in the present interim summary report.

Phase II and Phase III of this contract were funded at NASA Lewis Research Center through the Turbine Engine Hot Section Technology (HOST) project.

INTRODUCTION

Computational procedures to predict combustion processes are being developed and refined by a number of researchers (e.g., see Ref. 1 and surveys in Refs. 2 through 5). These computational procedures predict the velocity, species concentration, temperature and reaction rate distributions within the combustor and are used to determine combustor liner heat load, engine performance (combustion efficiency), pollution emissions (reactant products) and pattern factor (temperature distribution at turbine inlet). Because most combustors of practical interest have turbulent flow, the calculation procedures include mathematical models for the turbulent transport of mass (or species), momentum and heat. However, the prediction of combustion processes with improper turbulent transport models results in inaccurate predictions of combustor efficiency, linear heat load, emissions and exit temperature pattern factor.

The recent prediction of recirculating combusting flows, typical of those found in aircraft gas turbines, have produced qualitative results which "provide insight in to the nature of the combustion process rather than quantitative design information" (e.g., Ref. 1). Although the insight is helpful in diagnosing problems, the long term goal of the combustion designers is to decrease combustor development costs by using accurate combustor flow prediction procedures. The deficiencies in the current computational procedures have been attributed to weaknesses in both the mathematical models, including the turbulent transport models, and in the numerical methods. The recommendation from workshops and studies on combustion modeling are that the mathematical models used in the calculation procedures be validated using experiments specifically designed to provide the required initial conditions (e.g. Ref. 1). The first step in this process is the validation of the mass and momentum turbulent transport models for the less complicated constant density flow.

The data used to formulate and validate the turbulent transport models have been obtained primarily from velocity and momentum transport measurements because only a limited amount of concentration and mass transport data is available. The mass (species) transport data presently available are not sufficient to determine where inadequacies exist in the present models or to formulate improvements for the models. One reason for this situation is that the methods for simultaneously obtaining turbulent mass (species) and momentum transport data often have been indirect, requiring compromising assumptions. To overcome these limitations a technique was developed at UTRC to simultaneously measure concentration and velocity, and therefore, obtain mass transport data which can be used to evaluate and improve combustion oriented turbulent transport models for scalars such as concentration of species and temperature. The combined laser velocimeter laser induced fluorescence measurement technique was used to under Contract NAS3-22771

to obtain mass and momentum turbulent transport data with nonswirling and swirling confined coaxial jets (Refs. 6 and 7). These data have been used to evaluate computational procedures for predicting combustion processes at NASA Lewis (Ref. 5) and by the contractors in the 1982-83 NASA Lewis Hot Section Technology (HOST) Aerothermal Modeling Program (e.g. Ref. 8).

Although extensive measurements of velocity, concentration and turbulent transport rates were presented in Refs. 6 and 7, the length scales and dissipation rates were not measured. This deficiency in the measurement of all inlet conditions required for the computational procedures, leaves an opening in the comparison of predictions using various mathematical models and the experiments. The importance of inlet boundary conditions has been noted by several authors (e.g., Ref. 8) to be important in detemining the quantitative accuracy of the calculation procedure. The length scale and dissipation rate measurements, obtained in the present study, provide (a) the additional data required as inlet boundary conditions for the computational fluid mechanics codes and (b) measurements in the interior regions of the flowfields that can be compared directly with results of numerical predictions or the details of current or proposed turbulent transport models.

A problem was also encountered in comparing the experimental momentum transport results of Ref. 6 with the previous experimental results of Ref. 9 in that the center jet tube at the coaxial jet inlet used in Ref. 6 was tapered whereas that of Ref. 9 was blunt. The blunt trailing edge geometry apparently produced a different turbulent transport process which was more easily predicted by the current turbulent transport models, Ref. 10. Turbulent transport measurements were obtained in this phase of the present study to determine if differences occured due to the inner jet inlet geometry. However, the results for the blunt inlet presented in this report will show small differences compared to the results for the tapered inlet configuration presented in Ref. 6.

LENGTH SCALE AND DISSIPATION RATE MEASUREMENTS

A measurement technique was developed under UTC (UTRC and PWED) sponsorship to obtain length scale and dissipation rate measurments using a computerized data acquisition and reduction system. The measurement technique is applicable for flows where Taylor's hypothesis applies. The dissipation rate is calculated using an isotropic flow assumption. The small disturbance relationships will also be used to determine approximate eddy dissipation rates and length scales in regions where the approximation no longer applies in a strict sense. The approximate dissipation rate determined with the small disturbance relationship in regions with moderate turbulence intensity is likely to be reasonably good because the largest contribution to the dissipation rate occurs in the small eddies previously shown to be essentially isotropic. Additional effort will be required to determine the influence of higher turbulence intensities on the accuracy of the integral length scales.

Description of Measurement Technique

Mathematical Relationships

The relationships used to determine the eddy dissipation rate and the integral length scales are developed from isotropic turbulence theory and are regarded as "well established" by the fluid mechanics community. The form and nomenclature of the relationship was taken directly from Hinze (Ref. 11).

The spatial velocity gradients required to determine the dissipation rate are obtained by assuming that the temporal and spatial derivative at a point are related by $\partial/\partial t(\quad) = -U\partial/\partial x(\quad)$. In the strict sense, the relationship is good if the fluctuating velocity is much less than U, i.e. $u'/U \ll 0.01$. A well defined mean velocity, U, is also required. This requirement is most often satisfied when the turbulence intensity requirements is met. This approximation is known as Taylor's hypothesis.

The autocorrelation for time delay, τ, is defined

$$R(\tau) = \overline{u(t)\, u(t+\tau)}/u'^2$$

An integral scale of turbulence, an approximate microscale of turbulence and an eddy dissipation rate are related to the autocorrelation of the streamwise velocity fluctuations. The integral scale of turbulence is defined:

$$L1 = U \int_0^\infty R(\tau)\, d\tau$$

A second integral scale of turbulence is also obtained directly from the velocity fluctuation spectrum data and defined (Ref. 11):

$$L2 = (U/4)\ \lim_{f\to 0}\left[E(f)/u'^2\right]$$

The microscale length of turbulence, λ, is defined as the intercept (at $R(\tau)=0$) of the parabola that matches $R(\tau)$ for small τ, i.e.,

$$R(\tau) = 1 - (\tau U/\lambda)^2 = 0$$

where E(f) is the turbulent kinetic energy per frequency cycle of one velocity component at frequency f. The dissipation rate, ε, is related to the microscale of turbulence, the rms velocity and the fluid kinematic viscosity:

$$\varepsilon = 15\ \nu u'^2/\lambda^2_g = 30\ \nu u'^2/\lambda^2_f$$

where λ_f is a microscale length in the streamwise direction, λ_g is a microscale length in the crossstream direction. As noted earlier, this expression is a result of the isotropic assumption.

Although the autocorrelation/microscale relations shown above will lead to a dissipation rate, the determination of the curvature of $R(\tau)$ at $\tau=0$ is often difficult and sometimes ambiguous. Another relationship for the microscale is obtained more easily from the one-dimensional velocity turbulent energy spectra (Ref. 11):

$$1/\lambda_f^2 = (2\pi)/(U^2u'^2) \int_0^\infty dn\ n^2E(n)$$

In the opinion of the authors, the approximate dissipation rate is more easily and accurately obtained with the integral of an independent spectrum measurement rather than the double differentiation of experimental autocorrelations at $\tau = 0$.

It should be noted that the definitions of the integral scale and microscale from the correlator or from the spectrum are equivalent. An autocorrelation,

$R(\tau)$, is constructed from the Fourier transform of the energy spectral distribution using a computer routine which is part of the data reduction program. The Fourier transform which produces the spatial correlation is

$$R(\tau) = \int_0^\infty \cos(\omega\tau) E(\omega)\, d\omega$$

since both $R(\tau)$ and $E(\omega)$ are real. This autocorrelation is equivalent to that obtained using a correlator.

Velocity Measurement

Hot film/hot wire anemometry was used to measure the instantaneous streamwise velocity of the flow. A TSI model 1050 constant resistance anemometer was used with TSI model 1220-20 and 1210-20W hot wire and hot film probes in air and water, respectively, to produce an analog signal. The instantaneous heat transfer from the probe wire/film is obtained with conventional heat transfer relationships

$$\tilde{E}_1^2/R = \tilde{Q}_{wire} = \tilde{h}\,(T_w - T_f)\pi d\ell$$

where $\tilde{h} \approx (k/d)\left(A+B(\rho\tilde{u}d/\mu)^{0.5}\right)$. A TSI model 1057 linearizer was used to produce an instantaneous voltage proportional to the "instantaneous" stream wire velocity at the probe. Thus

$$\tilde{E}_2 = \bar{E}_2 + \tilde{e}_2 = C*\tilde{U} = C*(\bar{U} + \tilde{u}) \qquad (1)$$

where ~ and - denote instantaneous and time average values respectively. In all these expressions, the contributions of velocity components parallel to the sensor are assumed negligible.

A Spectral Dynamics Micro FFT Analyzer was used to obtain the spectrum of $\tilde{E}_2$ using conventional techniques. The Spectral Dynamics Micro FFT Analyzer has six frequency ranges with full range scales with maximum frequencies from 500 to 20,000 Hertz. Each frequency range is divided into 400 equally spaced increments. For the instrumentation development tests with air, the 0-20 KHz range was used. However, for the length scale experiments in water, the 0-1 KHz, 0-2 KHz or 0-5 KHz scales were used. Table II contains a listing of the components used in the length scale measurement technique.

Data Acquisition and Reduction Program

Although the mathematical relationships for the turbulence micro and integral length scales, the anemometer, and spectrum analyzer have been available for sometime, the amount of effort required to produce a length scale measurement is considerable. Limiting factors have been (a) the manual transfer of data from a spectrum analyzer to the data reduction computer and (b) the mathematical conversion of the spectral energy information to the autocorrelation function. Therefore, only a limited number of length scales have been determined from velocity spectra to date. The current availability (a) of electronic data transfer links between measurement instruments like the SD FFT Spectrum Analyzer and a microcomputer and (b) efficient fast Fourier transform algorithms for minicomputers makes the "production" measurement of length parameter feasible. The technical staff at UTRC recognized the need for the length scale information, the current availability of the electronic data transfer procedures and have implemented the procedures. The information flow chart for the data acquisition and reduction program is shown in Fig. 1. The first comprehensive set of data obtained at UTRC with the technique is that described in this report.

Spectral Dynamics FFT Spectrum Analyzer

The voltage spectrum, $E_3(I)$, is calculated from

$$E_3(I) = \left(V_{rms} * 10^{\,dB(I)/20}\right)^2/(1.5\ \Delta f)$$

for I=1 to 400. Here, dB(I) is the analyzer output, V_{rms} is the selected reference voltage, and Δf is the frequency step. All these data are entered directly through the interface during data acquisition. Note that the quantity (1.5 Δf), represents the effective analyzer filter bandwidth provided in the analyzer manual (Ref. 14). Data analysis is based on the assumption that the spectrum is essentially constant in the range, f to f + Δf.

Fast Fourier Transform

An important part of the data acquisition and reduction program is the fast-Fourier transform (FFT) program used to convert the input spectrum information to an autocorrelation. The technique is commonly used in other scientific disciplines and is discussed in Ref. 12. The FFT program employed was originally developed by Cooley and Tukey (Ref. 13). Basically, it involves a processing of the input data such that the number of calculations requires is significantly reduced (from N^2 to N log N where N is the number of points in the input data). One requirement of the FFT procedure used in the present application is that N be representable by

$$N = 2^M \qquad (2)$$

where M is any integer. In its present form, the FFT program is used to calculate the autocorrelation, using input spectrum data. The spectrum data is obtained as digital output from the Spectral Dynamics Spectrum Analyzer. The input data consists of voltage levels, $E_3(I)$, at 400 frequency intervals, Δf. To satisfy the requirement of Eq. (2), the spectrum input is assumed to be zero for frequency steps 401 through 512. This extension had no effect on the resulting maximum correlation time; it is still given by

$$\tau_{max} = 1/(2\Delta f).$$

A side benefit, however, is that the resulting autocorrelation is defined with 512 timesteps rather than 400 and is thus better defined. Within the spectrum thus defined, the next step in the analysis is the previously discussed FFT conversion of the velocity spectrum to an autocorrelation. With the noted addition of $E(I)= 0$ for $I=401$ to 512, the output is a 512 step autocorrelation $R(\tau)$ for $\tau=\tau_I$ defined by

$$\tau_I = (I-1)/(1024\ \Delta f)$$

$I = 1$ to 512.

Note two things: for $\tau=0$, $R(\tau)=1.0$ for the autocorrelation; and as mentioned earlier, $\tau_{max} = 1/(2\Delta f)$.

Data Analysis Program

The fluctuating voltage spectrum is converted to a fluctuating velocity spectrum $\tilde{E}(I)$ with the linearized output of (1); this simple transformation is given by

$$E(I) = (1/C)^2\ E_3(I).$$

The final portion of the data analysis procedure involves calculation of additional statistical properties. The mean-square turbulence intensity is calculated from

$$\overline{u^2} = \int_0^\infty E(f)df = \sum_{I=1}^{400} E(f)\Delta f$$

The microscale is calculated from

$$\lambda_f^2 = \frac{U^2}{2\pi^2} \frac{\int_0^\infty E(f)df}{\int_0^\infty f^2E(f)df} = \frac{U^2}{2\pi^2} \frac{\sum_{I=1}^{400} E(f)\Delta f}{\sum_{I=1}^{400} f^2E(f)\Delta f}$$

where λ_f is the microscale. The integral scale, L, is calculated in two ways; first, from the autocorrelation function,

$$L1 = \bar{U} \int_0^\infty R(\tau)d\tau = \bar{U} \sum_{i=1}^{400} R(\tau)\Delta\tau$$

or, given the Fourier transform relationships, the integral scale can be calculated from

$$L2 = \bar{U}/(4\bar{u}^2)\ \lim_{f\to o} E(f);$$

Finally, the dissipation rate, ε, is calculated from

$$\varepsilon = 30\ \nu\ \overline{u^2}/\lambda_f^2$$

Discussion of Results

Nonswirling Flow with Tapered Inlet

The length scale and dissipation rate measurements were conducted in the UTRC coaxial flow facility (Fig. 2) using water as the working fluid. The flow conditions and geometries were identical to those employed in Ref. 6, i.e. $\bar{U}$ (inner) = 0.52 m/s and $\bar{U}$ (annular) = 1.66 m/sec and with a Reynolds number of 35,000 based on the duct diameter and the average velocity. A sketch of the inlet and measurement locations is shown in Fig. 3. The swirler was not installed for the measurements discussed in this subsection. Mean, fluctuating and spectral measurements of the axial velocity were obtained in the regions without recirculation at z = -41, 5, 51 and 102 mm from the inlet plane. Mass and momentum turbulent transport data were obtained at the last three locations during Phase I (Ref. 6).

The mean and fluctuating axial velocity measurements obtained with the hot film anemometer at the four axial locations, are presented in Figs. 4 and 5, respectively, and compared with results from Ref. 6, obtained with a laser velocimeter. The agreement between the two sets of measurements is excellent. The conclusion from this comparison is that the hot film data acquisition and reduction procedure for obtaining mean and fluctuating velocities reproduces the previous results with acceptable accuracy.

The dissipation rate distributions for the four axial locations are presented in Fig. 6. Note the dissipation rates at the center of the inner jet and the annular jets are approximately the same at z = -41 and 5 mm from the inlet plane. At z = 5 mm, the dissipation rate across the inlet varies by 2 1/2 orders of magnitude. This radial variation decreases to less than one order of magnitude (by increasing the lower dissipation rates and decreasing the higher dissipation rates) at z = 102 mm from the inlet plane. Note however that there is a two order of magnitude range in the dissipation rate at z = 51 mm (2 in). As expected, the locally high and low dissipation rates are associated with high and zero axial velocity shear rates, respectively. It should be noted that the sensor length is slightly larger than the estimated Kolmorgorov scale, η. Since the dissipation is centered around η, a smaller sensor or a suitable correction will be required to obtain precise dissipation rates from the spectrum directly.

The integral length and micro scales of turbulence are presented in Fig. 7. The integral scales L1 and L2 were both determined as part of the computerized data reduction procedure. Note that the integral scales determined by both methods are generally in good agreement. The largest difference between the two scales is about 20 percent and occurred at z = 102 mm. This is a location with long wave length eddies occurring over a moderate frequency range. The differences between the two integral length scales are generally less than ten percent

with the integral scale determined from the integration of the auto correlation always being greater. The integral scales of turbulence in the inner jet inlet (z = -41 mm) were 9 to 12 mm, approximately half the tube diameter and compatible with length scales reported in Ref. 11 for previous work by Laufer.

The micro scales of turbulence, λ_f, were 15 to 40 percent of the integral length scales. The ratio of micro scale to integral scale inside the inlet duct (z = -41 mm) was somewhat greater than measured by Laufer for a two-dimensional duct, i.e.: 15 percent of the UTRC circular duct diameter compared to 10 percent of the Laufer 2-d slot height. Thus, the present results in the duct appear to be reasonably compatable with previous studies. The micro scale of turbulence does not vary much ($1<\lambda_f<3.8$ mm) compared to the integral scale of turbulence. For the two measurement locations downstream of the inlet, the ratio of the maximum to minimum microscales ($2<\lambda_f<4$ mm) is only half the ratio of the integral length scales ($4.2<L<19$).

Swirling Flow with Tapered Inlet

The length scale and dissipation rates were also measured 5 mm (0.2 in) downstream of the inlet plane with the swirler (used in Ref. 7) in the annular duct as shown in Fig. 3. The hot film probe axis was in the plane perpendicular to the probe traverse direction and parallel to the inlet plane. This caused the hot film probe to be most sensitive to the axial and radial velocity components and relatively insensitive to the tangential velocity components. This hot film axis orientation was chosen to maintain a small probe volume cross section in the radial direction where the peak velocity gradients occur. The consequences of this probe orientation on the results are not fully understood at this time. For those flow conditions with negligible radial velocities, the signal is primarily due to the axial velocity. In swirling flow, the fact that the sensor is parallel to the swirl reduces its influence on the signal. The approximations used to acquire and reduce the data for the nonswirling flow condition were also used for the swirling flow condition.

The mean axial velocity profiles measured at z = 5 mm (0.2 in) with the hot film and laser velocimeter (Ref. 7) are shown in Fig. 8a. The axial velocity measured with the hot film downstream of the inner jet was slightly less than that measured with the laser velocimeter. However the axial velocity measured with the hot film downstream of the annular jet almost coincides with the laser velocimeter measurements.

The fluctuating axial velocities (Fig. 8b) measured with the hot film at the centerline ($r/R_o = 0$) downstream of the inner jet and downstream of the central region of the annular stream ($r/R_o \approx 0.35$) are approximately equal those measured with the laser velocimeter. However, the fluctuating velocities measured with the hot film in the shear layers were as much as a factor of two greater than the laser velocimeter results. Some of these discrepancies are probably caused by the high turbulence intensities, u'/U, and the accompanying

velocity probability density distribution functions which include negative velocities and large crossflow velocities from the probe mounts into the sensor.

The dissipation rate distribution at z = 5 mm are presented in Fig. 9a. The dissipation rate downstream of the inner jet is approximately the same as for the nonswirling flow condition, as expected. However, the dissipation rate downstream of the central position of the annular duct with swirling flow is more than one order of magnitude greater than for the nonswirling flow condition (Fig. 6). The peak dissipation rates in the shear layers between the inner and outer streams and between the outer stream and the recirculation cell are approximately the same as for the nonswirling flow condition. The authors believe these measurements should be repeated with additional probe orientations before final conclusions regarding the differences between the swirling and nonswirling inlet conditions are reached.

The integral and microscales measured are presented in Figs. 9b and 9c, respectively. The microscale downstream of the inner jet inlet are approximately the same as for the nonswirling flow condition. The microscales downstream of the annular jets are about 50 percent of the values for the nonswirling flow condition; this is comparable with the order of magnitude higher measured dissipation rates and turbulence levels that are 10 to 50 percent higher than for the nonswirling flow condition. The integral length scales downstream of the annular jet are also less than those for the nonswirling flow conditions. The integral scales downstream of the inner jet are about 30 percent greater than for the nonswirling flow conditions. This may be associated with the low frequency unsteadiness which occurred at the upstream end of the recirculation cell at z = 38 mm (1.5 in) (Ref. 6). These length measurements experiments with the swirling flow condition have produced interesting results which most likely show general cause/effect relationships. However, the experiments were exploratory and the results need to be verified with additional measurements.

TURBULENT TRANSPORT EXPERIMENTS WITH BLUNT INNER JET INLET CONFIGURATION AND NONSWIRLING FLOW CONDITION

The mass and momentum turbulent transport experiment with nonswirling confined coaxial jets, previously conducted with a tapered inner jet inlet configuration (Ref. 6) was partially repeated using a blunt inner jet inlet configuration. This experiment was repeated in an attempt to resolve the apparent differences in the momentum turbulent transport process between the Johnson-Bennett experiment (Ref. 6) and The Habib-Whitelaw experiment (Ref. 15). Both experiments were conducted with coaxial jets discharging into an enlarged axisymmetric duct. Both experiments had the outer (annular) jet velocity higher than the inner (axisymmetric) jet velocity. In the Johnson-Bennett experiment, the centerline velocity was approximately constant with increasing axial distance from the inlet indicating the streamwise momentum of the inner jet was not rapidly transported to the wake region between the flow from the inner jet and the annular stream. In the Habib-Whitelaw experiment, the centerline velocity decayed appreciably downstream of the inlet plane before being accelerated by the annular jet. One identifiable difference between the two experiments was the inner jet inlet configuration with a blunt inlet configuration used in the Habib-Whitelaw experiment using a tapered inner jet inlet configuration used in the Johnson-Bennett experiment.

The experiment with nonswirling confined coaxial jets and the inner jet blunt inlet configuration will be discussed in the following subsections. Only small differences in the velocity, concentration and momentum turbulent transport results between the current and previous (Ref. 6) experiment were measured. The results from the current experiment did not resolve the previously stated dilemma. However, the previous results (Ref. 6) have been verified and data has been obtained at an additional axial location near the inlet region where changes in the transport process are more rapid.

Description of Test Apparatus

The facility and measurement techniques used in this experiment are identical to those used in Refs. 6 and 7. The test section was modified after the Ref. 7 experiment to facilitate cleaning and to be useable for the length scale and dissipation rate measurements. Description of the apparatus from Ref. 7 are presented in this section for completeness.

A schematic of the coaxial flow facility used in this experimental program is presented in Fig. 2. The principal components of the facility are a water storage tank, a water transfer and metering system, a dye injection system, and a test section. For the laser velocimeter tests, the facility was run in a closed,

recirculating loop. Water, which was at a temperature of approximately 20 C, was circulated by a pump from the storage tank, through metering valves and flow measuring devices to the inner jet and annular jet inlets of the inlet plenum. The water in the annular duct and inner tube entered the test section, mixed and discharged into the exhaust ducts, and was returned to the storage tank.

Whenever fluorescein dye was used as a tracer, such as for the flow visualization tests and the LV/LIF tests, the facility was operated in a single pass mode. The water from the exhaust ducts were discharged into the city sanitary sewer and fresh water replenished the system. For the flow visualization tests, dye was added to either the inner jet fluid or the annular jet fluid several feet upstream of the entrance to the test section to ensure uniform flow of dye into the test section. For the LV/LIF tests, uniform flow of the dye was ensured by adding the dye to a mixing chamber located a short distance from the dye micrometering valve. The 20 to 40 psi pressure drop across the valve was large compared to the other pressure drops in the system, thus ensuring a constant flow of the dye injected into the inner jet flow. The mixing chamber was large enough to ensure adequate mixing and a uniform dye concentration at the entrance of the test section. A magnetic rotating mixer was used in the dye reservoir to keep the dye well stirred and an inline filter was placed in the system to prevent clogging of the dye micrometering valve.

A sketch of the test section is shown in Fig. 3. The test section was a 122 mm inside diameter by 1 m long, thin-wall glass tube. When flow visualization and optical experiments are conducted in circular tubes, the water-glass-air interfaces can produce optical distortion. As shown in Fig. 2, the circular duct test section was enclosed in a rectangular, glass-walled optical box filled with water to reduce beam direction distortion as the laser beams passed from air through the glass wall of the duct and into the test section water. A ray tracing program was used to determine that the radial displacement of the probe volume was less than 0.03 mm and the offset of the measurement direction from radial was less than 0.05 deg for radii up to approximately 55 mm.

Water to the test section entered through an annular duct and a smaller inner jet tube. The water then exhausted through the exit duct, up over a weir and flowed to the drain. The top end of the exit duct containing the weir was open to the atmosphere to prevent the test section from becoming overpressurized. The inlet plenum for the annular duct contained three perforated plates to produce uniform flow and a honeycomb section to remove swirl from the flow. The inner jet tube was fed with the same diameter hose for lengths of over 300 cm and included a 60-cm length of straight, nonflexible tubing. A perforated plate was also positioned immediately upstream of the 60-cm tubing.

With this test section, measurements were usually made at a fixed axial location over a range of radial locations. The measured parameters discussed in

this report are presented as functions of the radial position r, normalized by the radius of the test section, R_o, i.e., r/R_o. For this representation, the inner jet tube extends from $r/R_o = 0.0$ to $r/R_o = 0.20$ and the annular region containing the swirler extends from $r/R_o = 0.25$ to $r/R_o = 0.48$. The inner and annular regions are separated by a thin wall which extends from $r/R_o = 0.20$ to $r/R_o = 0.25$. The region between $r/R_o = 0.48$ and $r/R_o = 1.0$ is a solid wall which acts like a backward facing step in the flow field.

Description of Laser Velocimeter and Laser Induced Fluorescence Measurement Techniques

The measurement techniques and equipment used for this experiment are identical to those used in Ref. 7. Description of the measurement techniques from Ref. 7 are presented in this section for completeness.

Overview

The laser velocimeter (LV) and laser induced fluorescence (LIF) measurements were obtained using commercially available components. Some electronic components, which were not commercially available when first required at UTRC, were designed and fabricated by the UTRC instrumentation group. The equipment utilized for each measurement will be described as the technique is discussed.

The LV measurement system employed in these experiments is sketched in Fig. 10 and utilized the two-color LV optics system detailed in Fig. 11. The two-color LV concept utilizes the two strong laser lines of an argon ion laser at 0.4880 μm (blue) and 0.5145 μm (green) wavelengths. These two colored beams are separated in the optical system and subsequently emitted as three beams; a blue beam, a green beam, and a 50-50 mixed blue/green (cyan) beam. The three beams are passed through a lens to produce two sets of orthogonal interference fringe patterns in one common focal volume each having a fringe spacing:

$$d_f = \lambda/(2 \sin(\theta/2)) \qquad (1)$$

where λ is the wavelength of the incident light beam, and θ is the intersection angle between the cyan beam and either the blue or green beam. A particle passing through the probe volume will scatter light of both colors, blue and green. The light intensity at the photomultiplier is modulated by a frequency, f_D, corresponding to the particular wavelength and fringe spacing and velocity component. This frequency is related to a particle velocity component through

$$f_D = U_i/d_f \qquad (2)$$

where U_i is the velocity component perpendicular to the optical axis and in the plane of one set of intersecting colored beams. More detailed descriptions of the particular two color laser Doppler velocimetry system utilized in this experiment including the frequency shift used to prevent flow direction ambiguity may be found in Ref. 16.

Two Component LV Measurements

For the measurements described in this report, the optical system was operated in a direct backscattering mode as shown in Fig. 10. The 0.4880 μm wavelength beam was used to measure the streamwise or axial velocity component, U. The 0.5145 μm wavelength beam was used to measure (a) the azimuthal velocity component, W, when the probe volume was moved horizontally across the stream and (b) the radial velocity component, V, when the probe volume was moved vertically. A Bragg cell was used for both velocity components to eliminate the flow direction ambiguity. This optical subsystem provided signal-to-noise ratios greater than 20 except near the test section walls. For the measurements made in this study, the nominal value of the beam intersection angle, θ, was 9.52 deg. The laser beam diameter was 1.25 mm and the beam separation at the 1.94:1 beam expander output lens was 53.5 mm. A 310 mm focal length achromatic lens was used to focus the beams. With these optical system parameters, the LV probe volume was calculated to have dimensions of 0.08 mm diameter, 1.01 mm length and contained 28 fringes.

Besides the sending and receiving optical subsystems, each LV system contains other components or subsystems which perform specific functions in the flow measurement. These include: (1) a scattering particle generator or seeder, (2) a traverse system to position the probe volume, (3) signal processors, and (4) a data handling subsystem. For the experiments performed for this study, the particles naturally occurring in the city water supply proved adequate as LV seeds. As indicated in Fig. 10, the traverse system consisted of a milling machine base having three directions of motion. The range of motion in the streamwise direction was approximately 240 mm while the ranges in the vertical and cross stream directions were greater than the dimension of the test section. The relative traverse position accuracy of this traverse system was approximately 0.1 mm.

Laser Doppler velocimeter (LDV) signal processors amplify and filter the signals from the multiplier tubes, validate the Doppler frequency samples, and finally compute the Doppler period which is the reciprocal of the Doppler frequency. The SCIMETRICS Model 800A signal processors used in this study

measured the elapsed time for 8 Doppler cycles and recorded the pulses from a 125 MHz crystal during the 8 cycle period. The processor also measured and recorded pulses for 4 and 5 Doppler cycles, and compared them with the 8 cycle result to ensure that the LDV signal was a valid one-particle signal. The integer number transmitted to the data handling system is the period of the Doppler frequency in nanoseconds. Two signal processors were used in this study (one for each colored light signal).

Once the LDV signals were processed and accepted, a microcomputer handing system was used to acquire, store and reduce the data. This system consisted of (1) a data handling interface (constructed in-house), (2) a DEC PDP 10/11 minicomputer with a dual disk operating system, (3) a DEC Laboratory Peripheral System (LPS) with an analog to digital (A/D) signal converter, and (4) a DECwriter III teletype printer. The LDV Data Handling Interface was used to accept only those data points for which the two velocity components were obtained within a period of time of 1 msec. This time period was considered appropriate for the probe volume length of approximately 1 mm which was used in this study and for typical velocities of 1 m/sec. Data acqusition rate tests conducted under this criteria indicated that almost all of the sets of two component velocity data were obtained from a single particle moving through the probe volume. A detailed listing of the equipment employed for the two velocity component LV measurements is presented in Table III.

Combined LV/LIF Measurements

The tracer dye used for the LV/LIF measurmements was made from fluorescein disodium salt ($C_{20}H_{10}O_5Na_2$). This dye is used extensively for water pollution studies and is available from chemical supply houses in powder form. Absorption and emission spectra data for fluorescein dye can be obtained from Ref. 17. A liquid dye concentrate was produced by dissolving 2.5 gms of dye powder in 1 liter of water to which was added 1 tablespoon of alcohol in order to stabilize the solution. A dilute solution of dye made by uniformly diluting 1 ml of concentrate with 3.5 liter of water was mixed "inline' with the inner jet fluid in the ratio of 1 part dilute solution to 760 parts water. Any variation in dye concentrations at the inner jet inlet location can be attributed to this last mixing process.

The 0.4880 μm wavelength beam of the argon ion laser was used in the LV/LIF experiment both to induce fluorescence of the fluorescein dye for the LIF measurement and to scatter light from particles for the LV measurements. Fluctuations in the laser beam intensity were monitored in bench tests to determine power fluctuations. The peak to peak power drift over a 20 minute period was less than 0.5 percent. The signal from the photomultiplier was filtered with a 2 kHz low pass filter to remove the shot noise associated with photomultiplier

tubes. The 2 kHz filtering was compatible with the typical velocity of 1 m/sec and probe volume length of 1 mm. The current signal was converted to a voltage, amplified and then processed through an A/D voltage converter each time an acceptable LV signal was obtained. The LV and LIF data were stored as pairs along with the data acquisition time by the Data Handling subsystem. A list of additional equipment used for the LV/LIF measurements is also presented in Table III.

Foreword To Presentation of Results

The use of computerized data acquisition, storage, reduction and analysis techniques permitted numerous quantities to be determined from the data obtained in this study in addition to the mean and fluctuating velocity components and concentrations usually obtained. These included (1) parameters which can be used to characterize the probability density functions of the velocity components, the concentrations, and the momentum transport rates and (2) the correlation coefficients for the transport process.

The determination of all possible parameters and correlations obtainable from the experimental data was beyond the scope of this study. However, the most universally used quantities have been calculated and are included in this report. The parameters presented include the mean value and three central moments of the velocity and concentration probability density functions (i.e., rms variation from the mean, skewness and kurtosis or flatness factor), the mean value and three central moments of the momentum turbulent transport rate probability density functions, and the correlation coefficients for the momentum turbulent transport rates. These parameters are defined in Table I.

The data point sets which are presented in this report were obtained for Flow Condition 1 of Ref. 6 and consist of single point measurements which were usually made at a fixed axial location over a range of radial locations. A data acquisition run number was assigned to each group of single point measurements. A new run number was assigned to each data point set each time a change in axial location or change in measured parameter was made; i.e., velocity component or concentration. The number of velocity/velocity or velocity/concentration data pairs which were acquired during each single point measurement was either 250, 500, or 1000 depending upon the number of particles traversing the probe volume. During data acquisition, all data was stored on floppy disks. This data was subsequently reduced to obtain the calculated parameters listed in the previous paragraph. The number of data pairs actually used in the data reduction was usually less than the 250, 500 or 1000 data pairs acquired because data pairs were eliminated during data reduction whenver spurious data was encountered. Spurious data was defined as data noncontiguous to and outside of the 3σ region of the probability density functions and was believed to occur when the laser velocimeter signal processor passed "bad" data because multiple or very large

particles passed through the probe volume or data was taken in regions of low signal-to-noise ratio.

All the calculated parameters obtained for each data acquisition run are presented in this report in tabular form. The mean and fluctuating velocity and concentration results and the turbulent momentum transport rates and correlations coefficient results are also presented in graphical form to aid in the discussion of the results. A listing of the run numbers from which data was utilized for the tables and figures presented in this report is presented in Table IV. The tabulated parameters for each data point set are tabulated in Tables V-XX where the term XX denotes the run number.

Discussion of Results

Velocity

The mean axial velocity profiles are presented in Fig. 12. The closest axial location to the inlet for which both velocity and concentration profiles could be obtained was 13 mm (0.5 in.). This location is approximately five inner jet tube wall thicknesses downstream from the inlet plane. Note that the velocity deficit caused by the boundary layers on the ID and OD of the inner jet inlet duct has been partially filled in at this axial location. The centerline velocities at all axial locations are close to those measured in Ref. 6. Small differences in the profiles occur at other radial locations. However, these differences are less than the scatter band measured in Ref. 6 for each profile. The mean radial profiles are presented in Fig. 13. The present results are also within the scatter of the data presented in Ref. 6.

The fluctuating axial and radial velocity profiles are presented in Figs. 14 and 15, respectively. The results are very similar to those presented in Ref. 6.

Momentum Turbulent Transport

The momentum turbulent transport rate data and the correlation coefficients are presented in Figs. 16 and 17. In general, the results from Ref. 6 and the present measurements data lie in the scatter band of the other set. The present set of results has less asymmetry than the Ref. 6 results. Data was also obtained closer to the outer test section wall in the present experiment than for Ref. 6. The correlation coefficient, R_{uv}, are also close to the Ref. 6 results. Differences between the present and Ref. 6 experiments occurred (1) where the turbulent transport rate is near zero and turbulent intensities are relatively low and thus the uncertainty is R_{uv} is high and (2) at z = 152 and 203 mm at the edge of the recirculation zone where asymmetries are likely to occur.

Inner Jet Fluid Concentrations

The mean and fluctuating inner jet concentrations are presented in Figs. 18 and 19. The mean concentration profiles are essentially the same as those previously measured (Ref. 6). The scatter bands for the two sets of data overlap for all axial stations. The fluctuating concentration results are similar to those previously measured with the major differences occurring at z = 13, 51, and 102 mm. At z = 13 mm, the present inner jet concentration fluctuations are lower at r/Ro = 0 due to improved uniformity of the inner jet fluid concentration at the inlet plane; f' = 0 is desired at z = 0 mm and r/Ro = 0.0. A noticable increase in f' occured at z = 13 mm and r/Ro = 0.2 to 0.25 compared to Ref. 6. Modest increases in f' also occured at z = 102 and r/Ro < 0.1; however f' is essentially the same for 0.1 < r/Ro < 0.3 where the largest amount of mass turbulent transport occurs. The conclusion from this comparison is that although the concentration fluctuations are increased at several locations, the mean concentration distribution is essentially the same for both the blunt and tapered inlet configurations.

SUMMARY OF RESULTS

Quantitative studies were conducted of the flow downstream of nonswirling and swirling coaxial jets discharging into an expanded duct. The ratio of annular jet diameter and duct diameter to the inner jet diameter were approximately 2 and 4, respectively. The inner jet peak axial velocity was approximately one-half the annular jet peak axial velocity. For the swirling flow condition, the mean swirl angle in the annular stream was approximately 30 degrees.

A computerized length scale measurement technique was used to determine the eddy dissipation rate and two integral length scales at selected locations in the test section for the nonswirling and swirling flow condition. Following are the principal results for the nonswirling flow conditions (for which the most extensive measurements were obtained):

1. The mean and rms fluctuating velocities measured using the hot film anemometer employed in the length scale measurement technique were approximately the same as those previously obtained using laser velocimeter measurement techniques.

2. The microscale and integral scales of turbulence measured in the inner jet inlet tube upstream of the inlet plane were approximately the same as those measured by other researchers.

3. Results showed that the eddy dissipation rates varied by 2 1/2 orders of magnitude near the inlet plane, by 2 orders of magnitude 51 mm (2.0 in.) from the inlet plane, and by 1 order of magnitude 102 mm (4 in.) from the inlet plane.

4. The ratio of the integral scale length to the microscale length varied from 2 to 6 depending upon radial and axial location in the test section.

5. The largest integral scale lengths (15-18 mm) occurred in the large eddy shear region between the annular stream and the recirculation cell. These wavelengths were compatable with those previously observed in flow visualization studies.

Velocity, concentration and momentum turbulent transport rates were measured downstream of a blunt inner jet inlet configuration for the nonswirling flow condition. These measurements were obtained to compare with previous results obtained downstream of a tapered inner jet inlet configuration.

6. The mean and fluctuating velocity and concentration profiles and the momentum turbulent transport rate profiles were essentially the same as those previously measured for the blunt inner jet inlet configurations.

REFERENCES

1. Gerstein, M. (Ed.): Fundamentals of Gas Turbine Combustion, NASA Conference Publication 2087, 1979.

2. Hudson, D. A.: Combustion Modeling Needs for the '80s. AIAA Preprint 80-1288.

3. Mellor, A. M.: Turbulent-Combustion Interaction Models for Practical High Intensity Combustors: Seventeenth Symposium on Combustion, p. 377, Combustion Institute, 1979.

4. Dryburgh, D. and R. B. Edelman: Technical Evaluation Report on the Propulsion and Energetics Panel 54th Meeting on Combustion Modeling. AGARD Advisory Report No. 153, March 1980.

5. Mularz, E. J.: New Trends in Combustion Research For Gas Turbine Engines. NASA Technical Memorandum 83338. AVRADCOM Technical Report 83-C-1, June 1983.

6. Johnson, B. V. and J. C. Bennett: Mass and Momentum Turbulent Transport Experiments with Confined Coaxial Jets, NASA Contractor Report CR-165574, November 1981.

7. Roback, R. and B. V. Johnson: Mass and Momentum Turbulent Transport Experiments with Confined Swirling Coaxial Jets, NASA Contractor Report CR-168252, August 1983.

8. Sturgess, G. J.: Aerothermal Modeling. Phase I. NASA Contractor Report Contractor Report CR-168202, May 1983.

9. Habib, M. A. and J. H. Whitelaw: Velocity Characteristics of Confined Coaxial Jets With and Without Swirl. ASME Journal of Fluids and Engineering, Vol. 102, pp. 47-53 (1980).

10. Syed, S. A. and G. J. Sturgess: Velocity and Concentration Characteistics and Their Cross Correlations for Coaxial Jets in a Confined Sudden Expansion - Part II: Predictions. Fluid Mechanics of Combustion Systems, ASME 1981, p. 161-168.

11. Hinze, J. L.: Turbulence, McGraw-Hill, 1959.

12. Cooper, J. W.: The Microcomputer in the Laboratory: With Examples Using the PDP-11. John Wiley and Sons, New York, 1983.

REFERENCES (Cont'd)

13. Cooley, J. W. and J. W. Tukey: An Algorithm for the Machine Computation of Complex Fourier Series (FFT), Mathematics of Computations, Vol. 19, 1965.

14. _____: Model SD340 Micro FFT Analyzer Operator's Handbook, 1977.

15. Habib, M. A. and J. H. Whitelaw: Velocity Characteristics of a Confined Coaxial Jet. ASME J. of Fluids Engineering, Vol. 101, p. 522-529, December 1979.

16. DISA 55X Modular LDA Optics-Instruction Manual. DISA Information Department; DISA Electronics.

17. _____: Kodak Laser Products. Kodak Publication No. JJ-169, March 1972.

18. Tennekes, H. and J. L. Lumley: A First Course in Turbulence, Chapter 6. MIT Press, 1972.

TABLE I

DEFINITIONS OF SEKWNESS AND KURTOSIS FOR VELOCITY, CONCENTRATION, AND TRANSPORT PROBABILITY DENSITY FUNCTIONS

Terms in this table for the velocity components and concentrations are defined using the rotation of Ref. 18 and conventional statistical methods.

$\tilde{u}$	Local instantaneous axial velocity component
$B(\tilde{u})$	Probability density function (p.d.f.) of $\tilde{u}$ with properties $B(\tilde{u}) \geq 0$ and $\int_{-\infty}^{\infty} B(u)\, du = 1.0$
U	Mean value of axial velocity component defined: $U = \int_{-\infty}^{+\infty} \tilde{u}\, B(\tilde{u})\, d\tilde{u}$
u	Local instantaneous axial velocity fluctuation from the mean, defined: $u = \tilde{u} - U$
σ_u or u'	Second central moment of velocity u defined: $\sigma_u^2 = u'^2 = \int_{-\infty}^{-\infty} u^2\, B(\tilde{u})\, d\tilde{u}$ Will also be denoted as rms fluctuation.
$\overline{u^n}$	nth central moment of velocity u defined: $\overline{u^n} = \int_{\infty}^{\infty} u^n\, B(\tilde{u})\, d\tilde{u}$
S_u	Skewness of velocity component, u, p.d.f. defined: $S_u = \overline{u^3}/\sigma_u^3$
K_u	Kurtosis (or flatness factor) of velocity component, u, p.d.f. defined: $K_u = \overline{u^4}/\sigma_u^4$

In like manner, the mean, rms fluctuation, skewness, and kurtosis for the radial velocity, azimuthal velocity and concentration are defined.

The second moments, skewness and kurtosis for the momentum and mass transport rates are defined in a similar manner.

uv	Local instantaneous momentum turbulent transport rate: $(\tilde{u}-U)(\tilde{v}-V)$
$B(uv)$	Probability density function (p.d.f.) of uv with properties $B(uv) > 0$ and $\int_{-\infty}^{+\infty} B(uv)\, d(uv) = 1.0$
$\overline{uv}$	Mean value of turbulent momentum transport rate defined: $uv = \int_{-\infty}^{\infty} (\tilde{u}-U)(\tilde{v}-V)\, b(uv)\, d(uv)$
$(uv)'$	Local instantaneous fluctuation of momentum transport rate from mean, defined: $(uv)' = uv - \overline{uv}$

σ_{uv} Second central moment of momentum transport rate: $\sigma_{uv} = \int_{-\infty}^{\infty} (uv)'^2 \, B(uv) \, d(uv)$

$(uv)^n$ nth central moment of momentum transport rate: $(uv)^n = \int_{-\infty}^{\infty} (uv)'^n \, B(uv) \, d(uv)$

S_{uv} Skewness of momentum transport rate: $S_{uv} = (\overline{uv})^3/\sigma^3_{uv}$

K_{uv} Kurtosis of momentum transport rate: $K_{uv} = (\overline{uv})^4/\sigma^4_{uv}$

In a like manner, the mean, second central moment, skewness and kurtosis for the momentum transport in the r-z plane and the mass transport in three directions are defined.

TABLE II

COMPONENTS USED IN LENGTH SCALE MEASUREMENT TECHNIQUE

Hotwire Equipment

TSI Constant Resistance Anemometer

. 1210 - 20 w	Hot film sensor
. 1050	Constant Temperature Anemometer
. 1052	Signal Linearizer
. 1051 - 20	Monitor and Power Supply

Spectrum and Correlator

Spectral Dynamics Model SD340
Micro FFT Analyser

- IEE 488 (talk only) modification

SAICOR Model 42
Correlator and Probability Analyser

Computer

DEC PDP 11/23S

- IEE 488 interface board
- Parallel interface board

TABLE III

COMPONENTS USED IN LV AND LV/LIF MEASUREMENT SYSTEM

I. Laser Light Source

Argon Ion Laser (Spectra Physics Model 164)
- TEM_{00} mode
- All lines, 1.0 watt power
- 0.4880 um wavelength, 0.5 watts power

II. LV Optics

DISA Type 55x00 Two Color LDV System
- Polarization rotator
- Beamsplitter - Module I
- Bragg Cell, 1 mHz effective frequency offset
- Beamsplitter - Module II
- Backscatter Section - 04880 um wavelength filter and photomultiplier tube
- Backscatter Section - 0.5145 um wavelength filter and photomultiplier tube
- Pinhole Section
- Beam Translator
- Beam Expander
- Achromatic lens, 310 mm focal length

III. Electronics

LV Signal Processor (SCIMETRICS Model 800A)
- 2 units
- 0.4 to 2.0 mHz range
- 3% data window
- 4/8 and 5/8 comparison for "good signals"

Oscilloscope (Tektronics Model 465B)
- 2 units

LV Data Handling Interface (UTRC design)
- Clock
- Coincidence check

Minicomputer (DEC PDP 11/10)
- Floppy disk
- DECwriter III (1200 baud rate)

IV. LIF Electronics

Low Pass Filter (Kronhite Model 3202)
- 2KHz

Voltage Amplifier (Preston 8300 XWB Amplifier - Model A)
- 1-1000X Amplification

A/D Converter (DEC LPS11)
- Computer controlled

Digital Voltmeter (Hewlett Packard Model 3465A)

High Voltage Power Supply (Fluke Model 415B)
- 0-2500 volts

TABLE IV

TABLE OF RUN NUMBERS FROM WHICH DATA WAS UTILIZED FOR TABLES AND FIGURES

Measured Parameters	Axial Location, z - mm (in.)					
	12.7(0.5)	25.4(1.0)	50.8(2.0)	101.6(4.0)	152.4(6.0)	203.2(8.0)
U, V, uv	6,7	9	10	11	12	13
U, C			18	19	20	21
V, C	24,30		25	26	27	28

TABLE V-6

AXIAL AND AZIMUTHAL VELOCITY DATA AND CORRELATIONS

Test Date: 3/7/84 Run No.: 6 Flow Condition: 1 Geometry: 3

Axial Location: 13 mm (0.5 in.) $x/R_o = 0.208$

Pt No.	r mm +(θ=0) -(θ=180)	r/R_o	U m/s	u' m/s	S_u	K_u	W m/s	w' m/s	S_w	K_w	$\overline{uw}$ m^2/s^2	R_{uw}	σ_{uw} m^2/s^2	S_{uw}	K_{uw}	N
1	16.2	.265	1.597	.182	-1.534	9.07	-.093	.108	-.320	5.89	-.00147	-.075	.026	.76	44.98	994
2	19.2	.315	1.647	.081	-.537	5.49	-.055	.063	.232	3.57	-.00034	-.067	.006	-1.27	20.21	998
3	22.3	.365	1.633	.077	-.242	6.69	.025	.067	-.014	3.47	.00010	.019	.006	-.05	10.65	996
4	25.3	.415	1.633	.076	-.590	6.13	.048	.060	-.193	4.53	.00033	.107	.005	1.75	31.80	997
5	28.4	.465	1.435	.185	-.863	4.21	.033	.128	.012	4.52	.00152	.068	.026	.43	15.75	996
6	31.4	.515	.526	.301	-.341	2.57	-.003	.253	-.094	3.66	-.00674	-.074	.083	.07	7.10	994
7	13.1	.215	.627	.228	.271	3.92	.045	.237	.051	3.99	.00199	.037	.059	-.28	16.24	998
8	10.1	.165	.661	.103	-.100	2.49	.018	.060	-.028	3.03	-.00010	-.015	.007	-.87	10.27	466
9	7.0	.115	.779	.092	-.091	3.07	.016	.053	-.279	3.03	-.00041	-.085	.005	-.31	8.19	470
10	4.0	.065	.869	.075	.071	3.63	.007	.043	.161	3.16	-.00019	-.059	.003	-.04	8.56	477
11	.9	.016	.866	.072	.082	3.36	.010	.040	.144	3.08	-.00036	-.125	.003	-.93	9.49	477
12	11.6	.190	.598	.123	-.252	3.43	.020	.088	.286	6.46	-.00022	-.020	.012	.72	18.97	474
13	14.7	.240	1.207	.285	-.763	4.67	.000	.247	.403	4.18	-.00853	-.121	.079	-1.66	19.81	993
14	34.5	.565	-.093	.155	-.997	7.11	-.045	.186	.853	6.76	-.00019	-.007	.023	.13	8.17	247
15	37.5	.615	-.085	.141	-.385	4.19	-.060	.179	1.579	8.84	.00046	.018	.023	1.29	9.81	246
16	43.6	.715	-.098	.160	-.473	5.41	-.076	.137	.044	2.61	-.00031	-.019	.020	.40	7.52	239
17	49.7	.815	-.028	.118	-.712	3.09	-.105	.124	.668	3.94	-.00043	-.029	.015	.37	7.69	245
18	-2.1	-.034	.821	.089	.088	4.05	-.010	.043	-.235	3.43	.00037	.096	.004	1.66	14.55	486
19	-5.1	-.084	.774	.092	-.021	3.25	-.007	.052	-.141	2.99	.00051	.128	.005	.34	7.29	458
20	-11.2	-.184	.579	.108	-.255	2.87	.006	.073	-.199	4.55	.00033	.105	.008	.29	7.20	471
21	-12.8	-.209	.584	.213	.463	4.34	-.023	.183	-.252	5.05	-.00212	-.054	.039	-.75	13.60	993
22	-14.3	-.234	.956	.276	.234	2.81	-.015	.249	-.232	3.46	.00080	.012	.070	.45	11.58	999
23	-17.3	-.284	1.594	.107	-.729	4.02	.027	.071	-.156	3.77	.00220	.287	.009	2.27	17.36	997
24	-20.4	-.334	1.622	.066	-.536	7.94	-.036	.054	.064	3.45	.00011	.031	.004	.96	15.26	997
25	-23.4	-.384	1.645	.054	-.975	6.49	-.056	.043	-.174	3.94	.00022	.095	.003	2.58	43.84	999
26	-26.5	-.434	1.565	.111	-1.050	5.50	-.045	.071	.281	4.07	-.00053	-.080	.008	-1.05	13.47	998
27	-29.5	-.484	1.074	.252	-.267	2.59	-.020	.172	.031	3.44	.00309	.071	.044	1.18	14.07	499
28	-32.6	-.534	.072	.234	.502	4.41	-.022	.222	-.378	3.41	-.00015	-.003	.061	-2.44	24.54	496

TABLE V-7

AXIAL AND RADIAL VELOCITY DATA AND CORRELATIONS

Test Date: 3/8/84 Run No.: 7 Flow Condition: 1 Geometry: 3

Axial Location: 13 mm (0.5 in.) $x/R_o = 0.208$

Pt No.	r mm +(θ=0) -(θ=180)	r/R_o	U m/s	u' m/s	$S_{u'}$	$K_{u'}$	V m/s	v' m/s	$S_{v'}$	$K_{v'}$	$\overline{u'v'}$ m^2/s^2	$R_{u'v'}$	$\sigma_{u'v'}$ m^2/s^2	$S_{u'v'}$	$K_{u'v'}$	N
1	.0	.000	.848	.082	-.140	2.99	-.014	.046	.168	4.09	-.00052	-.140	.004	-1.52	10.27	485
2	-3.0	-.050	.822	.081	-.076	3.06	-.003	.043	.131	3.03	.00044	.126	.003	1.27	9.15	459
3	-6.1	-.100	.776	.082	-.049	3.27	-.010	.045	.188	2.94	.00052	.167	.004	.88	10.61	476
4	-9.1	-.150	.684	.095	-.293	3.09	-.022	.049	.023	2.86	.00077	.165	.005	.61	7.08	464
5	-12.2	-.200	.526	.129	.037	3.53	-.008	.138	-1.666	7.31	.00135	.376	.022	2.83	46.81	496
6	-15.2	-.250	1.286	.239	-.756	4.49	-.130	.173	.673	3.79	-.01695	-.407	.046	-2.27	13.41	997
7	-18.3	-.300	1.664	.075	-.752	7.61	-.080	.051	.353	3.89	-.00046	-.120	.004	-2.21	19.85	990
8	-21.3	-.350	1.667	.064	-.272	9.15	-.084	.046	-.135	3.38	.00036	.123	.003	1.04	11.22	995
9	-24.4	-.400	1.663	.084	-.494	5.73	-.056	.049	-.377	4.06	.00076	.186	.005	3.37	27.35	984
10	-27.4	-.450	1.483	.165	-1.384	8.57	-.038	.076	-.502	3.65	.00337	.270	.013	1.49	16.19	992
11	-30.5	-.500	.777	.268	-.418	4.06	-.032	.180	-.058	2.88	.02219	.460	.047	1.48	8.01	998
12	-33.5	-.550	-.026	.168	-.435	8.07	-.036	.086	.376	4.37	.00426	.294	.016	2.30	18.48	492
13	-36.6	-.600	-.057	.118	.031	5.39	-.037	.064	.227	3.37	.00043	.057	.008	.86	11.72	242
14	33.5	.550	-.038	.135	-.232	6.08	-.050	.086	.242	4.58	.00204	.176	.015	5.20	57.17	493
15	30.5	.500	.784	.293	-.379	3.49	-.048	.203	-.092	2.44	.02804	.471	.051	1.60	8.60	995
16	32.8	.537	.066	.202	.424	4.38	-.031	.152	.958	4.58	.01357	.442	.038	3.69	25.74	499
17	29.5	.483	1.134	.260	-.601	4.02	-.024	.166	-.469	3.49	.01691	.392	.049	2.24	15.05	995
18	25.9	.425	1.628	.085	-1.342	6.95	-.023	.052	-.853	4.96	.00146	.332	.006	4.18	33.76	998
19	22.9	.375	1.675	.046	-.819	24.05	-.030	.034	-.133	4.56	-.00012	-.081	.002	-2.17	33.81	999
20	19.8	.325	1.643	.060	-.926	8.95	-.035	.040	.713	5.91	-.00064	-.271	.003	-4.24	38.85	998
21	16.8	.275	1.447	.141	-.505	4.06	-.060	.097	.541	4.46	-.00491	-.369	.017	-3.55	27.04	999
22	13.7	.225	.677	.208	.116	3.58	-.141	.226	.135	2.81	-.01936	-.412	.050	-.62	12.07	992
23	10.7	.175	.655	.199	-2.789	12.79	-.032	.060	-.741	5.26	.00096	.072	.013	-2.39	37.90	489
24	7.6	.125	.806	.085	-.498	4.92	-.030	.046	-.297	3.20	.00070	.178	.004	1.45	9.45	486
25	4.6	.075	.849	.073	.056	3.30	-.029	.039	-.073	4.96	.00002	.008	.003	-.86	13.13	483
26	1.5	.025	.859	.086	-.155	3.77	-.020	.040	-.160	2.89	-.00044	-.128	.003	-.32	6.81	482
27	12.2	.200	.549	.168	-.383	7.09	-.049	.161	-1.340	5.28	.00156	.058	.025	-1.77	12.97	489
28	-42.7	-.699	-.055	.146	-.928	6.27	-.032	.089	.567	8.35	.00218	.168	.013	1.98	22.05	245
29	-48.8	-.799	-.089	.207	-1.348	6.21	-.027	.082	-.127	3.17	.00430	.235	.019	-.14	18.94	215

TABLE V-9

AXIAL AND RADIAL VELOCITY DATA AND CORRELATIONS

Test Date: 3/9/84 Run No.: 9 Flow Condition: 1 Geometry: 3

Axial Location: 25 mm (1.0 in.) $x/R_o = 0.416$

P_t No.	r mm +(θ=0) -(θ=180)	r/R_o	U m/s	u' m/s	S_u	K_u	V m/s	v' m/s	S_v	K_v	$\overline{uv}$ m^2/s^2	R_{uv}	σ_{uv} m^2/s^2	$S_{\mu v}$	K_{uv}	N
1	.0	.000	.828	.079	-.147	3.72	-.008	.050	-.025	5.22	-.00028	-.069	.005	-2.25	38.96	483
2	-3.0	-.050	.794	.089	-.185	4.39	-.006	.050	-.194	3.83	.00083	.185	.005	.99	9.97	484
3	-6.1	-.100	.767	.089	-.193	3.49	-.001	.049	-.254	3.19	.00089	.205	.005	1.25	13.38	464
4	-9.1	-.150	.669	.105	-.276	3.10	-.005	.069	-.741	5.84	.00133	.183	.009	-1.17	25.77	472
5	-12.2	-.200	.776	.190	-.200	5.82	-.007	.202	-.823	4.24	-.01450	-.379	.040	-1.62	10.96	499
6	-15.2	-.250	1.326	.208	-.524	2.94	-.003	.177	.466	3.69	-.01612	-.440	.040	-2.24	12.59	999
7	-10.7	-.175	.649	.129	.557	4.47	-.047	.127	-1.028	4.90	-.00328	-.200	.021	-4.62	50.30	962
8	-18.3	-.300	1.641	.075	-.438	7.42	-.075	.064	.790	5.11	-.00058	-.121	.007	-9.01	171.60	996
9	-21.3	-.350	1.634	.064	-.202	6.53	-.067	.050	-.135	3.74	.00046	.143	.003	.93	12.97	998
10	-24.4	-.400	1.604	.093	-.925	6.42	-.054	.065	-.511	3.91	.00156	.260	.008	4.12	36.78	999
11	-27.4	-.450	1.388	.195	-.810	4.33	-.013	.115	-.673	4.31	.00809	.360	.031	3.86	35.99	998
12	-30.5	-.500	.844	.265	-.184	3.40	.045	.190	-.328	3.64	.02259	.451	.052	1.94	14.20	999
13	-30.5	-.500	.787	.271	-.217	3.30	.031	.198	-.207	3.36	.02348	.437	.061	1.83	11.63	999
14	-33.5	-.550	.309	.239	-.109	3.90	.049	.182	.067	4.65	.01990	.457	.044	2.31	13.36	494
15	-36.6	-.600	-.055	.240	-.335	5.14	-.025	.136	1.184	6.46	.01223	.374	.052	.78	62.01	484
16	-42.7	-.699	-.090	.174	-.909	5.09	-.048	.081	-.150	3.00	.00179	.126	.016	-.92	16.77	497
17	-48.8	-.799	-.065	.219	.981	7.89	-.033	.098	-.131	6.42	.00209	.097	.020	.68	15.75	239
18	33.5	.550	.255	.282	-.264	3.10	.039	.211	.504	3.71	.02543	.428	.061	1.08	9.30	497
19	35.1	.575	.004	.272	-.440	4.98	-.007	.170	1.112	5.72	.01743	.377	.052	2.18	13.09	497
20	32.0	.525	.514	.268	-.035	3.24	.055	.202	-.256	3.11	.01941	.359	.059	-.01	15.26	997
21	29.0	.475	1.129	.269	-.381	3.29	.019	.190	-.383	3.04	.02297	.450	.055	1.33	11.28	999
22	25.9	.425	1.613	.109	-1.478	8.66	-.001	.078	-.583	4.19	.00254	.298	.012	5.42	58.73	998
23	22.9	.375	1.681	.049	-.451	15.35	-.005	.049	-1.250	11.56	.00032	.133	.003	9.91	217.70	999
24	19.8	.325	1.624	.060	-.999	12.61	.001	.049	.179	3.49	-.00071	-.243	.004	-3.37	31.13	999
25	16.8	.275	1.464	.141	-.809	4.14	-.039	.117	.955	5.05	-.00651	-.400	.022	-3.59	28.19	998
26	13.7	.225	.940	.185	.116	2.73	-.092	.180	.078	2.68	-.01484	-.445	.034	-.97	9.59	999
27	7.6	.125	.784	.095	.218	4.73	.014	.092	5.173	42.46	.00080	.092	.006	-.54	20.19	488
28	4.6	.075	.833	.080	-.037	3.67	.010	.052	-.451	4.55	.00004	.010	.005	2.24	21.81	487

R84-915540-34

TABLE V-10

AXIAL AND RADIAL VELOCITY DATA AND CORRELATIONS

Test Date: 3/9/84 Run No.: 10 Flow Condition: 1 Geometry: 3

Axial Location: 51 mm (2.0 in.) $x/R_o = 0.833$

P_t No.	r mm +(θ=0) -(θ=180)	r/R_o	U m/s	u' m/s	S_u	K_u	V m/s	v' m/s	B_v	K_v	$\overline{uv}$ m^2/s^2	R_{uv}	σ_{uv} m^2/s^2	S_{uv}	K_{uv}	N
1	.0	.000	.816	.078	.232	4.01	.009	.057	.070	3.62	-.00022	-.050	.004	-1.05	8.45	484
2	-3.0	-.050	.768	.083	-.167	3.28	-.003	.056	.197	3.47	.00029	.063	.005	.04	6.95	486
3	-6.1	-.100	.743	.109	.987	7.43	-.010	.065	.389	6.35	.00077	.109	.007	-.37	15.21	488
4	-9.1	-.150	.759	.132	.502	3.59	-.045	.124	-1.475	8.13	-.00532	-.326	.021	-3.17	25.11	495
5	-12.2	-.200	1.029	.192	-.015	3.64	-.077	.162	-.182	3.14	-.01157	-.373	.033	-.61	9.11	998
6	-15.2	-.250	1.376	.184	-.466	2.71	-.067	.150	.455	3.12	-.01210	-.439	.030	-1.63	9.48	999
7	-18.3	-.300	1.615	.084	-1.028	8.48	-.058	.082	.684	4.94	-.00091	-.133	.011	-5.81	61.86	999
8	-21.3	-.350	1.617	.072	-.679	8.09	-.047	.069	-.290	4.04	.00125	.251	.007	5.46	79.83	999
9	-24.4	-.400	1.567	.131	-1.237	6.82	-.026	.100	-.651	4.90	.00424	.323	.021	5.76	59.33	998
10	-27.4	-.450	1.283	.247	-.669	3.24	.013	.164	-.602	3.89	.01714	.424	.052	4.13	46.27	999
11	-30.5	-.500	.870	.288	-.033	2.78	.042	.207	-.159	2.93	.02717	.456	.055	1.58	8.11	999
12	-33.5	-.550	.500	.306	.016	3.48	.044	.217	.187	3.38	.03117	.469	.078	2.33	20.82	998
13	-36.6	-.600	.239	.308	-.167	3.07	.018	.196	-.101	5.36	.02526	.418	.074	3.36	33.99	993
14	-39.6	-.649	.010	.268	.371	2.63	-.015	.177	.150	10.31	.02006	.423	.064	6.80	77.36	492
15	-42.7	-.699	-.140	.280	-.619	6.50	-.042	.160	-.800	10.90	.01144	.255	.060	3.41	35.11	493
16	-48.8	-.799	-.114	.217	1.028	6.08	-.030	.112	.394	9.15	.00248	.102	.027	-1.49	24.27	240
17	32.0	.525	.639	.284	-.037	2.87	.044	.213	-.122	3.02	.02698	.445	.068	2.13	13.81	999
18	25.9	.425	1.470	.216	-1.244	5.40	.032	.143	-.688	4.41	.00939	.324	.037	1.40	17.40	996
19	22.9	.375	1.656	.081	-.699	8.78	.006	.085	-.741	5.62	.00225	.326	.010	4.08	49.57	995
20	19.8	.325	1.650	.066	-.506	7.30	-.005	.071	-.290	4.57	.00023	.050	.006	.67	20.01	999
21	16.8	.275	1.495	.152	-.913	4.04	-.028	.104	.607	3.68	-.00651	-.416	.020	-2.82	16.22	999
23	7.6	.125	.780	.161	-5.103	47.20	-.009	.075	-.995	4.85	.00173	.143	.017	9.75	148.00	492
22	10.7	.175	.889	.143	.434	3.58	-.053	.122	-.552	3.49	-.00704	-.405	.021	-2.97	25.49	991
24	13.7	.225	1.165	.198	-.104	3.09	-.049	.147	.084	2.92	-.01338	-.475	.029	-1.31	7.12	999

TABLE V-11

AXIAL AND RADIAL VELOCITY DATA AND CORRELATIONS

Test Date: 3/9/84 Run No.: 11 Flow Condition: 1 Geometry: 3

Axial Location: 102 mm (4.0 in.) $x/R_o = 1.665$

P_t No.	r mm +(θ=0) -(θ=180)	r/R_o	U m/s	u' m/s	S_u	K_u	V m/s	v' m/s	S_v	K_v	$\overline{uv}$ m^2/s^2	R_{uv}	σ_{uv} m^2/s^2	$S_{\mu v}$	K_{uv}	N
1	.0	.000	.857	.139	.972	5.50	-.008	.107	-.533	6.99	-.00037	-.025	.024	.38	26.69	493
2	-3.0	-.050	.850	.144	1.233	6.19	-.049	.136	-1.660	9.14	-.00439	-.225	.030	-4.73	52.59	495
3	-6.1	-.100	.892	.192	-.041	7.18	-.064	.134	-.887	5.96	-.00820	-.319	.032	.53	39.75	994
4	-9.1	-.150	1.018	.188	.469	2.96	-.067	.139	-.271	3.11	-.01182	-.452	.028	-1.82	10.80	999
5	-12.2	-.200	1.199	.212	.004	2.42	-.063	.144	-.056	3.01	-.01356	-.448	.029	-1.10	5.64	999
6	-15.2	-.250	1.409	.188	-.490	2.91	-.060	.139	-.072	4.26	-.00973	-.373	.028	-1.77	12.02	997
7	-18.3	-.300	1.552	.154	-.940	4.14	-.041	.134	-.161	4.63	-.00098	-.048	.029	1.78	31.74	992
8	-21.3	-.350	1.569	.167	-1.481	6.90	-.007	.143	-.528	6.04	.00554	.233	.044	2.73	52.53	997
9	-24.4	-.400	1.459	.236	-1.106	4.24	.019	.165	-.666	4.83	.01456	.376	.056	4.65	36.58	998
10	-27.4	-.450	1.239	.295	-.657	3.44	.041	.200	-.350	3.92	.02544	.432	.054	2.00	11.34	998
11	-30.5	-.500	1.037	.312	-.435	3.23	.073	.206	-.207	3.57	.02237	.348	.066	1.60	10.84	994
12	-33.5	-.550	.745	.337	-.353	3.48	.050	.241	.014	3.62	.03312	.407	.083	1.66	14.32	994
13	-36.6	-.600	.564	.367	-.260	3.30	.067	.245	.183	2.83	.03903	.434	.090	1.41	9.35	997
14	-39.6	-.649	.299	.385	-.029	2.72	.039	.239	.535	3.56	.03851	.420	.097	1.41	10.03	998
15	-42.7	-.699	.154	.371	.056	2.41	.010	.219	.215	5.11	.03492	.431	.086	2.64	20.96	996
16	-44.8	-.749	-.145	.282	1.038	4.29	-.035	.190	.125	6.25	.01572	.294	.057	2.56	26.56	480
17	45.7	.749	-.094	.317	.817	3.62	-.044	.168	.554	4.54	.01918	.361	.052	2.43	19.78	493
18	38.1	.624	.402	.408	-.185	3.44	.061	.257	-.351	2.97	.03814	.364	.107	.40	12.37	997
19	29.0	.475	1.034	.340	-.253	2.83	.061	.236	-.312	2.94	.03690	.460	.086	1.70	11.63	999
20	19.9	.325	1.586	.173	-1.696	8.86	.020	.153	-.514	5.11	.00679	.256	.045	6.38	65.77	999
21	13.7	.225	1.339	.210	-.280	2.87	-.046	.145	-.133	3.53	-.00958	-.315	.031	-.74	8.65	999
22	22.9	.375	1.496	.247	-1.435	5.62	.042	.185	-.707	4.39	.01657	.365	.055	4.30	41.33	999
23	51.8	.849	-.277	.234	1.040	8.11	-.035	.115	.260	5.02	.00553	.209	.036	5.04	72.72	485

TABLE V-12

AXIAL AND RADIAL VELOCITY DATA AND CORRELATIONS

Test Date: 3/12/84 Run No.: 12 Flow Condition: 1 Geometry: 3

Axial Location: 152 mm (6.0 in.) x/R_o = 2.498

P_t No.	r mm +(θ=0) -(θ=180)	r/R_o	U m/s	u' m/s	S_u	K_u	V m/s	v' m/s	S_v	K_v	$\overline{uv}$ m^2/s^2	R_{uv}	σ_{uv} m^2/s^2	S_{uv}	K_{uv}	N
1	.0	.000	.980	.208	-.458	2.77	-.008	.169	.010	4.38	-.00578	-.164	.036	-.22	12.86	493
2	.0	.000	.983	.239	-.950	6.97	-.006	.175	.119	4.35	-.00250	-.062	.043	.18	15.29	995
3	-3.0	-.050	.999	.247	-1.284	7.85	-.032	.161	-.170	3.61	-.00451	-.116	.040	-.03	13.85	989
4	-6.1	-.100	1.059	.237	-.628	5.57	-.063	.167	-.107	3.83	-.00878	-.222	.045	3.06	51.62	990
5	-9.1	-.150	1.111	.230	-.297	3.48	-.057	.165	-.240	3.07	-.01234	-.339	.038	.64	15.91	997
6	-12.2	-.200	1.223	.239	-.657	4.61	-.048	.159	-.390	3.54	-.01024	-.269	.037	2.03	32.68	998
7	-15.2	-.250	1.310	.240	-.925	5.14	-.039	.186	-.249	3.78	-.00071	-.016	.051	2.14	20.25	998
8	-18.3	-.300	1.356	.232	-1.004	4.74	-.006	.172	-.103	3.48	.00139	.047	.053	3.75	36.36	995
9	-21.3	-.350	1.377	.251	-1.092	5.26	.023	.194	-.419	3.84	.01042	.214	.056	4.31	43.17	997
10	-24.4	-.400	1.333	.284	-1.125	5.33	.054	.211	-.429	3.80	.01456	.245	.067	2.68	22.01	991
11	-27.4	-.450	1.205	.313	-.888	4.11	.092	.241	-.568	4.46	.02759	.365	.103	3.38	28.46	989
12	-30.5	-.500	1.017	.379	-.675	3.48	.091	.262	-.344	3.01	.03818	.384	.105	1.98	12.37	996
13	-33.5	-.550	.888	.409	-.750	4.14	.101	.279	-.331	2.85	.04886	.427	.125	1.54	12.44	996
14	-36.6	-.600	.730	.457	-.724	3.38	.101	.299	-.139	2.80	.05154	.378	.148	1.42	7.73	987
15	-39.6	-.649	.515	.510	-.799	3.56	.101	.293	-.013	2.99	.06208	.416	.141	.81	6.59	998
16	-42.7	-.699	.289	.540	-.435	2.87	.067	.302	.152	3.01	.05515	.399	.141	.41	6.14	498
17	-45.7	-.749	.047	.492	.300	2.24	.035	.256	.255	3.74	.05786	.458	.117	1.13	6.67	484
18	-48.8	-.799	-.046	.409	.629	2.86	.041	.256	.601	3.85	.04652	.445	.099	1.88	8.79	494
19	-51.8	-.849	-.219	.287	.983	3.40	-.005	.191	.748	4.17	.02144	.391	.069	1.50	12.02	244
20	-54.9	-.899	-.383	.292	.461	5.18	.003	.149	.579	4.94	.00355	.082	.053	-.66	15.92	233
21	38.1	.624	.576	.443	-.424	3.00	.120	.304	-.029	2.93	.05407	.401	.137	1.41	7.44	985
22	29.0	.475	1.109	.329	-.762	4.05	.125	.249	-.297	3.06	.02100	.257	.092	2.48	20.01	989
23	13.7	.225	1.285	.241	-.771	4.57	-.015	.182	-.375	3.88	-.00503	-.115	.047	.51	12.62	990
24	10.7	.175	1.203	.255	-.832	6.16	-.051	.182	-.411	3.92	-.00492	-.106	.057	5.36	68.59	988

TABLE V-13

AXIAL AND RADIAL VELOCITY DATA AND CORRELATIONS

Test Date: 3/12/84 Run No.: 13 Flow Condition: 1 Geometry: 3

Axial Location: 203 mm (8.0 in.) $x/R_o = 3.331$

Pt No.	r mm +(θ=0) -(θ=180)	r/R_o	U m/s	u' m/s	S_u	K_u	V m/s	v' m/s	S_v	K_v	$\overline{uv}$ m^2/s^2	R_{uv}	σ_{uv} m^2/s^2	S_{uv}	K_{uv}	N
1	1.3	.021	1.009	.247	-.971	5.98	.010	.194	.091	4.75	-.00353	-.076	.055	-.45	21.97	997
2	-1.8	-.029	1.088	.234	-1.139	7.02	.009	.191	.124	3.72	-.00134	-.030	.048	-.09	17.07	984
3	-4.8	-.079	1.085	.234	-.842	5.95	-.009	.183	-.018	3.84	-.00330	-.077	.044	-.85	16.98	981
4	-7.9	-.129	1.077	.262	-1.302	7.67	-.001	.182	-.261	3.59	-.00174	-.037	.060	3.31	43.05	993
5	-10.9	-.179	1.086	.249	-.704	4.41	.001	.202	-.381	4.54	-.00181	-.036	.052	-.04	39.93	991
6	-14.0	-.229	1.098	.262	-.513	3.38	.009	.190	-.158	3.59	.00008	.002	.051	1.25	12.02	996
7	-17.0	-.279	1.114	.268	-.806	4.79	.025	.199	-.506	3.60	.00570	.107	.054	2.68	21.00	998
8	-20.1	-.329	1.087	.292	-1.009	4.79	.066	.210	-.516	4.31	.00614	.100	.078	3.26	33.17	997
9	-23.1	-.379	1.070	.286	-.603	3.78	.081	.220	-.396	3.26	.01370	.218	.070	1.94	15.02	991
10	-26.2	-.429	.992	.325	-.956	5.15	.097	.222	-.210	3.45	.02081	.289	.088	3.06	19.66	996
11	-29.2	-.479	.905	.340	-.780	3.92	.097	.259	-.286	3.27	.02637	.297	.102	1.99	15.21	989
12	-32.3	-.529	.822	.354	-.451	3.25	.129	.269	-.270	3.15	.03698	.389	.107	2.43	14.35	993
13	-35.3	-.579	.736	.409	-.727	3.70	.146	.270	-.302	2.96	.03994	.362	.116	1.53	8.07	988
14	-38.3	-.629	.591	.421	-.509	2.87	.137	.284	-.258	2.84	.04527	.379	.125	1.35	6.89	984
15	-41.4	-.679	.472	.457	-.719	3.86	.146	.282	-.127	2.78	.05159	.400	.126	1.18	7.45	992
16	-44.4	-.729	.319	.423	-.185	2.40	.146	.290	.560	4.36	.04738	.387	.119	.15	11.36	993
18	-50.6	-.829	.019	.418	-.126	3.36	.083	.280	.252	3.45	.04379	.374	.094	.74	8.04	491
19	-53.6	-.878	-.051	.354	.763	3.23	.066	.241	1.307	6.41	.02651	.310	.081	1.74	12.21	236
20	42.4	.695	.471	.392	-.360	3.01	.126	.287	-.208	2.68	.04201	.373	.111	.93	5.35	990
21	33.3	.545	.767	.360	-.475	3.34	.108	.266	-.126	2.98	.03350	.351	.105	1.99	10.62	996
22	30.2	.495	.843	.339	-.561	3.23	.096	.260	-.269	3.07	.02729	.310	.100	2.09	12.85	998

TABLE V-18

AXIAL VELOCITY AND CONCENTRATION

Test Date: 5/23/84 Run No.: 18 Flow Condition: 1 Geometry: 3

Axial Location: 51 mm (2.0 in.) x/R_o = 0.833

Pt No.	r mm +(θ=90) -(θ=270)	r/R_o	U m/s	u' m/s	$S_{u'}$	$K_{u'}$	f	f'	S_f	K_f	$\overline{uf}$ m/s	R_{uf}	σ_{uf} m/s	S_{uf}	K_{uf}	N
2	.0	.000	.666	.049	-.148	3.00	1.013	.023	5.599	70.10						991
3	3.0	.050	.653	.056	-.301	3.60	.999	.025	-6.463	97.05						991
4	6.1	.100	.617	.076	.160	3.82	.944	.117	-2.169	7.86						991
5	9.1	.150	.769	.172	.589	2.82	.541	.196	.301	2.37						994
7	12.2	.200	1.092	.209	-.105	2.94	.372	.135	.647	3.85						998
8	15.2	.250	1.453	.183	-.852	3.82	.154	.095	.845	3.35						998
9	18.3	.300	1.591	.082	-.345	5.68	.034	.025	3.356	19.42						994
11	21.3	.350	1.587	.097	-.564	5.11	.011	.007	1.481	7.74						985
12	24.4	.400	1.495	.194	-2.249	10.51	.002	.004	.762	3.72						994
13	30.5	.499	.765	.319	-.329	3.49	.002	.004	.416	3.53						997
14	36.6	.599	.112	.311	-.076	2.70	.007	.005	.620	4.45						491
16	42.7	.699	-.117	.177	-.487	3.75	.009	.004	1.510	10.96						497
17	48.8	.799	-.158	.166	-.107	3.18	.010	.007	8.537	128.00						496
20	-6.1	-.100	.754	.072	-.046	3.06	.885	.102	-.651	4.24						942
22	-7.6	-.125	.732	.086	.236	3.81	.908	.147	-1.854	6.50						960
23	-9.1	-.150	.770	.121	.801	3.94	.701	.202	-.444	2.11						971
24	-10.7	-.175	.897	.174	.506	3.14	.493	.186	.338	2.51						982
25	-12.2	-.200	1.012	.216	-.337	4.73	.377	.162	.442	3.03						984
26	-13.7	-.225	1.193	.215	-.174	2.85	.264	.146	.966	4.62						991

TABLE V-19

AXIAL VELOCITY AND CONCENTRATION

Test Date: 5/31/84 Run No.: 19 Flow Condition: 1 Geometry: 3

Axial Location: 102 mm (4.0 in.) $x/R_o = 1.665$

Pt No.	r mm +(θ=90) -(θ=270)	r/R_o	U m/s	u' m/s	$S_{u'}$	$K_{u'}$	f	f'	S_f	K_f	$\overline{uf}$ m/s	R_{uf}	σ_{uf} m/s	S_{uf}	K_{uf}	N
5	.0	.000	.806	.106	1.309	8.01	.894	.219	-1.941	5.03						981
6	3.0	.050	.819	.123	.917	7.10	.819	.243	-1.109	3.18						984
7	6.1	.100	.905	.189	.259	4.66	.541	.253	.045	1.99						992
9	9.1	.150	1.061	.229	-.482	5.03	.466	.207	.507	2.93						994
10	12.2	.200	1.267	.223	-.444	3.73	.295	.165	.806	3.99						992
11	15.2	.250	1.447	.186	-1.084	4.71	.171	.132	1.254	5.21						988
12	18.3	.300	1.531	.152	-1.545	8.13	.067	.077	2.301	9.05						994
13	21.3	.350	1.483	.185	-1.497	6.12	.025	.036	3.983	24.27						999
14	24.4	.400	1.337	.253	-.964	3.56	.012	.017	4.781	30.45						997
15	27.4	.449	1.099	.334	-.789	3.83	.009	.018	5.179	32.70						999
16	30.5	.499	.877	.343	-.400	2.90	.007	.014	6.702	57.90						996
17	33.5	.549	.660	.363	-.600	3.74	.007	.011	8.371	98.98						499
19	36.6	.599	.514	.411	-.675	3.49	.008	.008	4.446	45.68						478
20	42.7	.699	.050	.358	.337	3.05	.013	.008	6.706	95.88						495
21	48.8	.799	-.173	.280	.652	3.14	.016	.007	1.800	9.68						496
26	-7.6	-.125	.938	.181	.684	3.31	.540	.242	.114	2.15						987
27	-10.7	-.175	1.158	.216	-.188	2.76	.312	.178	.599	3.15						981
28	-13.7	-.225	1.345	.186	-.653	3.36	.183	.138	.857	3.76						997

R84-915549-34

TABLE V-20

AXIAL VELOCITY AND CONCENTRATION

Test Date: 5/31/84 Run No.: 20 Flow Condition: 1 Geometry: 3

Axial Location: 152 mm (6.0 in.) x/R_o = 2.498

Pt No.	r mm +(θ=90) -(θ=270)	r/R_o	U m/s	u' m/s	$S_{u'}$	$K_{u'}$	f	f'	S_f	K_f	$\overline{uf}$ m/s	R_{uf}	σ_{uf} m/s	S_{uf}	K_{uf}	N
1	.0	.000	.941	.226	-.545	5.14	.432	.250	.609	2.65						986
2	3.0	.050	.951	.220	-.444	4.85	.437	.242	.632	2.64						982
3	6.1	.100	1.011	.263	-.975	6.47	.385	.215	.722	3.12						983
4	9.1	.150	1.133	.245	-.532	4.46	.319	.196	.885	3.81						984
5	12.2	.200	1.241	.234	-.532	3.31	.245	.180	1.093	4.47						985
6	15.2	.250	1.321	.230	-.743	3.35	.179	.158	1.458	5.70						983
8	18.3	.300	1.345	.224	-.845	4.02	.116	.121	1.754	7.24						993
9	21.3	.350	1.304	.251	-.909	3.85	.065	.086	2.880	14.54						993
10	24.4	.400	1.205	.291	-.772	3.56	.045	.075	3.922	21.84						994
11	27.4	.449	1.040	.342	-.817	3.84	.025	.037	5.265	37.91						989
12	30.5	.499	.879	.346	-.320	2.70	.019	.026	6.001	46.74						996
13	33.5	.549	.669	.399	-.643	3.42	.039	.043	3.803	21.99						995
14	36.6	.599	.514	.416	-.387	2.89	.034	.035	4.142	25.16						999
15	42.7	.699	.270	.415	-.058	2.42	.031	.027	7.280	83.54						494
16	48.8	.799	.016	.352	.519	2.75	.033	.016	3.013	20.67						494

TABLE V-24

RADIAL VELOCITY AND CONCENTRATION

Test Date: 6/14/84 Run No.: 24 Flow Condition: 1 Geometry: 3

Axial Location: 13 mm (0.5 in.) x/R_o = 0.208

Pt No.	r mm +(θ=0) -(θ=180)	r/R_o	V m/s	v' m/s	S_v	K_v	f	f'	S_f	K_f	$\overline{vf}$ m/s	R_{vf}	σ_{vf} m/s	S_{vf}	K_{vf}	N
2	.0	.000	-.010	.050	.290	4.82	1.001	.021	-1.624	1.34						890
3	-3.0	-.050	.018	.051	-.457	4.48	1.079	.021	-2.797	37.53						918
4	-6.1	-.100	.029	.051	-.703	7.05	1.086	.022	-2.125	-13.84						931
5	.0	.000	-.008	.054	.367	4.38	1.005	.034	-3.893	20.67						462
6	-9.1	-.150	.035	.059	-.364	3.89	1.078	.028	-3.839	17.23						920
7	-12.2	-.200	.056	.182	.935	7.15	1.001	.068	-2.109	8.97						965
8	-15.2	-.250	-.099	.213	.590	3.28	.217	.154	.836	3.27						997
9	-18.3	-.300	-.048	.058	.180	3.68	-.011	.001	-.129	2.80						998
10	-21.3	-.350	-.055	.054	-.134	3.45	-.006	.001	.050	2.91						994
11	-24.4	-.400	-.035	.061	-.010	4.01	-.006	.001	-.087	2.61						991
12	-30.5	-.500	.034	.180	-.069	3.28	.004	.005	8.337	165.80						997
13	-36.6	-.600	.018	.259	.998	6.49	.021	.004	.451	4.12						469
14	.0	.000	-.010	.060	.753	5.18	1.029	.031	-2.428	4.38						453
15	-13.2	-.216	-.053	.217	-.508	3.89	.038	.195	-1.303	4.54						991
16	-14.2	-.233	-.038	.244	-.046	2.90	.001	.226	-.001	2.11						992
17	-42.7	-.699	-.021	.089	.423	4.07	.016	.004	.487	2.80						179
18	.0	.000	-.025	.118	-2.919	15.91	1.002	.023	-1.814	-8.47						469
20	.0	.000	-.005	.057	.368	4.73	1.001	.021	-1.879	2.41						429
21	3.0	.050	-.007	.055	.092	5.19	1.045	.027	-2.066	11.27						871
23	.0	.000	-.010	.056	-.162	4.94	1.001	.032	-1.935	14.59						413
24	.0	.000	-.012	.058	.225	7.72	.999	.018	-.584	57.47						459
26	12.2	.200	-.018	.220	.581	10.37	.858	.153	-1.128	3.66						993
27	15.2	.250	-.139	.187	.476	4.30	.089	.085	.988	3.79						993
28	18.3	.300	-.087	.053	.619	4.42	-.010	.001	-.006	3.07						993
29	21.3	.350	-.080	.039	.279	4.10	-.008	.001	.291	4.73						994
30	13.2	.216	-.152	.264	-.597	4.56	.462	.195	.019	2.25						985
31	14.2	.233	-.150	.251	.202	3.30	.256	.156	.579	2.76						983
32	.0	.000	-.006	.065	.899	9.46	1.007	.015	-.344	-22.73						445

MASS AND MOMENTUM TURBULENT TRANSPORT EXPERIMENTS United Technologies Research Center/NASA Lewis Research Center (Contract NAS3-22771)

TABLE V-25

RADIAL VELOCITY AND CONCENTRATION

Test Date: 6/15/84 Run No.: 25 Flow Condition: 1 Geometry: 3

Axial Location: 51 mm (2.0 in.) $x/R_o = 0.833$

Pt No.	r mm +(θ=0) -(θ=180)	r/R_o	V m/s	v' m/s	S_v	K_v	f	f'	S_f	K_f	$\overline{vf}$ m/s	R_{vf}	σ_{vf} m/s	S_{vf}	K_{vf}	N
7	.0	.000	-.016	.070	-.411	5.49	1.037	.013	.000	-84.71						460
8	3.0	.050	-.016	.063	-.502	5.42	.911	.013	-.791	87.52						461
9	9.1	.150	-.076	.155	-1.823	7.84	.706	.214	-.251	1.99						982
10	12.2	.200	-.107	.165	-.626	4.50	.299	.128	.719	3.57						987
11	12.2	.200	-.086	.128	.611	4.13	.101	.068	.769	3.57						996
12	18.3	.300	-.061	.084	-1.217	14.05	.011	.031	3.527	16.80						997
13	21.3	.350	-.048	.082	-1.490	11.54	-.000	.003	12.720	265.50						997
14	3.0	.050	-.030	.102	-3.550	21.53	.305	.015	.068	-18.03						468
16	24.4	.400	-.030	.128	-.958	5.93	.001	.003	1.230	6.52						979
17	27.4	.450	.010	.203	-1.091	5.30	.004	.004	.855	4.40						983
18	30.5	.500	.027	.211	.050	3.43	.008	.004	.237	3.28						487
19	36.6	.600	-.022	.206	.643	6.37	.008	.005	9.516	159.20						495

TABLE V-27

RADIAL VELOCITY AND CONCENTRATION

Test Date: 6/19/84 Run No.: 27 Flow Condition: 1 Geometry: 3

Axial Location: 152 mm (6.0 in.) x/R_o = 2.498

Pt No.	r mm +(θ=0) -(θ=180)	r/R_o	V m/s	v' m/s	S_v	K_v	f	f'	S_f	K_f	$\overline{vf}$ m/s	R_{vf}	σ_{vf} m/s	S_{vf}	K_{vf}	N
2	.0	.000	-.074	.242	-1.855	10.23	.399	.210	.473	2.71						983
4	6.1	.100	-.054	.183	.279	4.57	.324	.195	.670	3.12						994
5	9.1	.150	-.066	.196	-.420	4.99	.276	.192	.917	3.71						991
6	12.2	.200	-.065	.222	-1.000	8.50	.186	.148	1.073	4.12						996
7	15.2	.250	-.039	.213	-.353	4.87	.121	.120	1.486	5.52						991
8	18.3	.300	.010	.218	.147	5.35	.088	.100	1.730	6.36						991
9	21.3	.350	.029	.240	-.285	4.91	.053	.081	2.536	10.26						999
10	24.4	.400	.060	.240	-.284	3.15	.032	.052	3.248	16.00						993
11	27.4	.450	.093	.239	-.169	2.98	.018	.030	4.523	29.74						990
12	30.5	.500	.097	.253	-.147	3.20	.017	.025	4.607	29.49						990
13	36.6	.600	.090	.273	.029	3.19	.012	.010	4.340	30.15						994
14	43.7	.716	.096	.309	.741	4.13	.009	.007	1.360	6.35						489
15	48.8	.799	.079	.319	1.791	8.57	.009	.006	.761	3.90						196
17	-6.1	-.100	-.021	.206	-.573	7.81	.367	.213	.713	3.13						995
18	-12.2	-.200	-.004	.170	.373	4.87	.252	.170	.898	4.00						988
19	-18.3	-.300	.026	.216	-.865	9.08	.130	.129	1.608	6.29						996
20	-24.4	-.400	.087	.216	-.316	4.49	.036	.064	3.282	17.15						994
21	-30.5	-.500	.109	.275	-.393	4.84	.017	.036	10.250	157.70						988

FIG. 1

INFORMATION FLOW CHART FOR COMPUTERIZED LENGTH SCALE MEASUREMENT TECHNIQUE

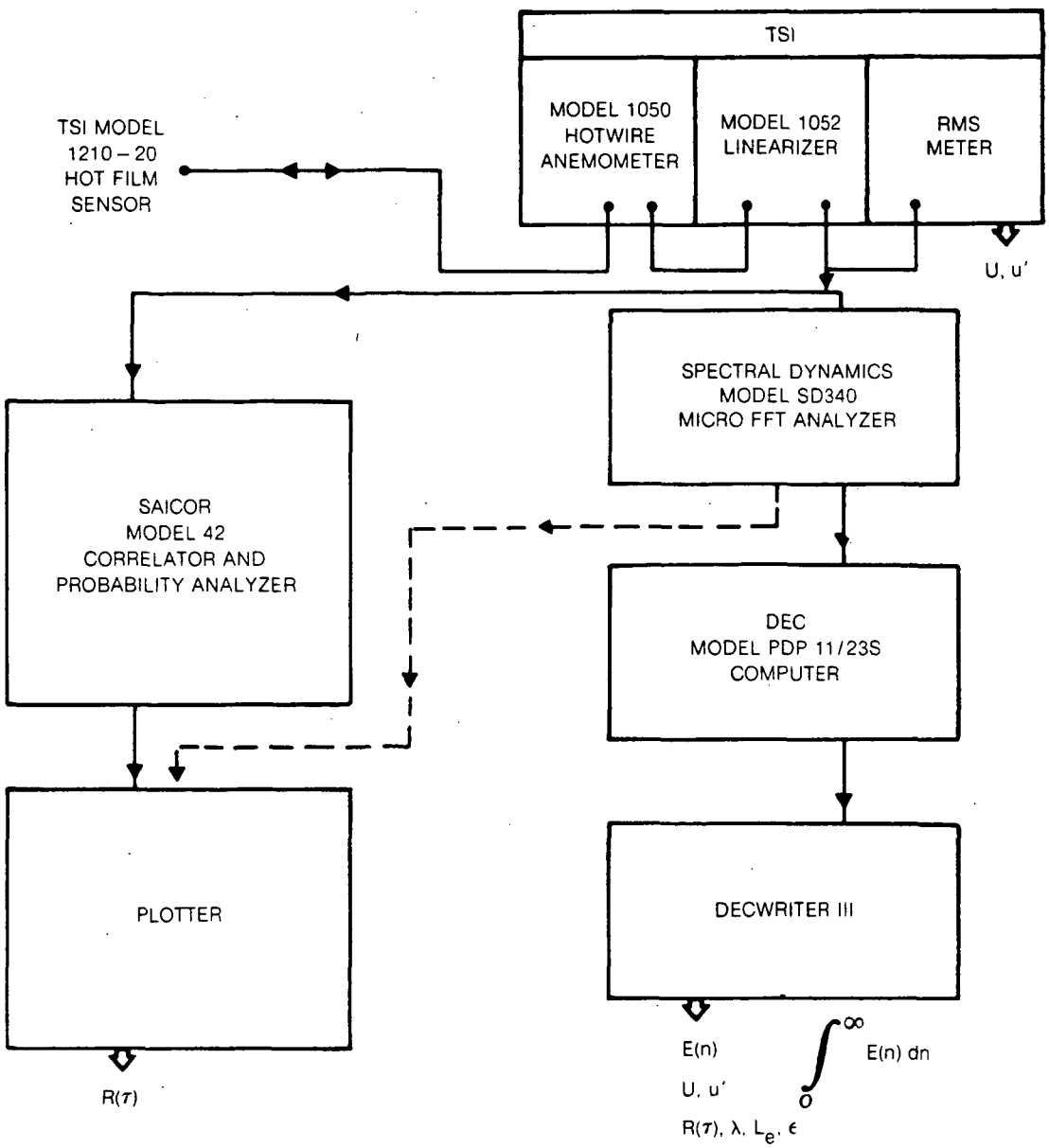

84-9-1-2

FIG. 2

SKETCH OF COAXIAL FLOW FACILITY

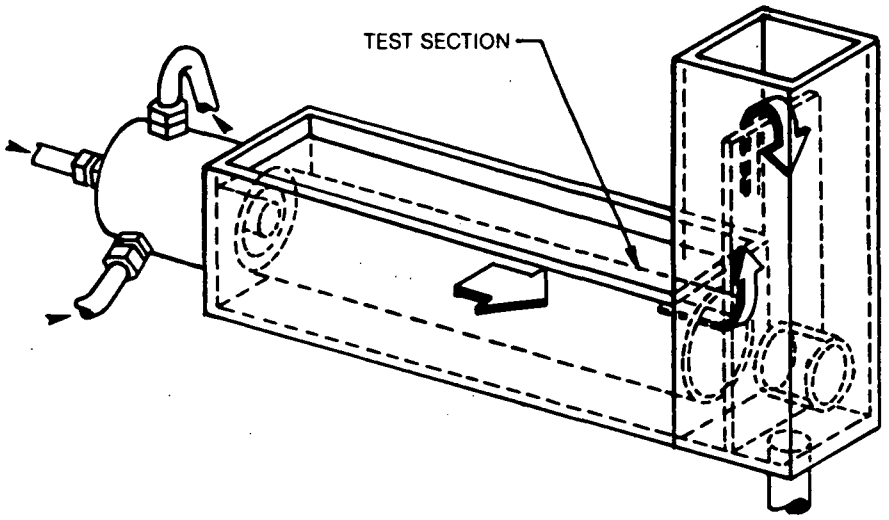

FIG. 3

SKETCH OF LENGTH SCALE MEASUREMENT ARRANGEMENT

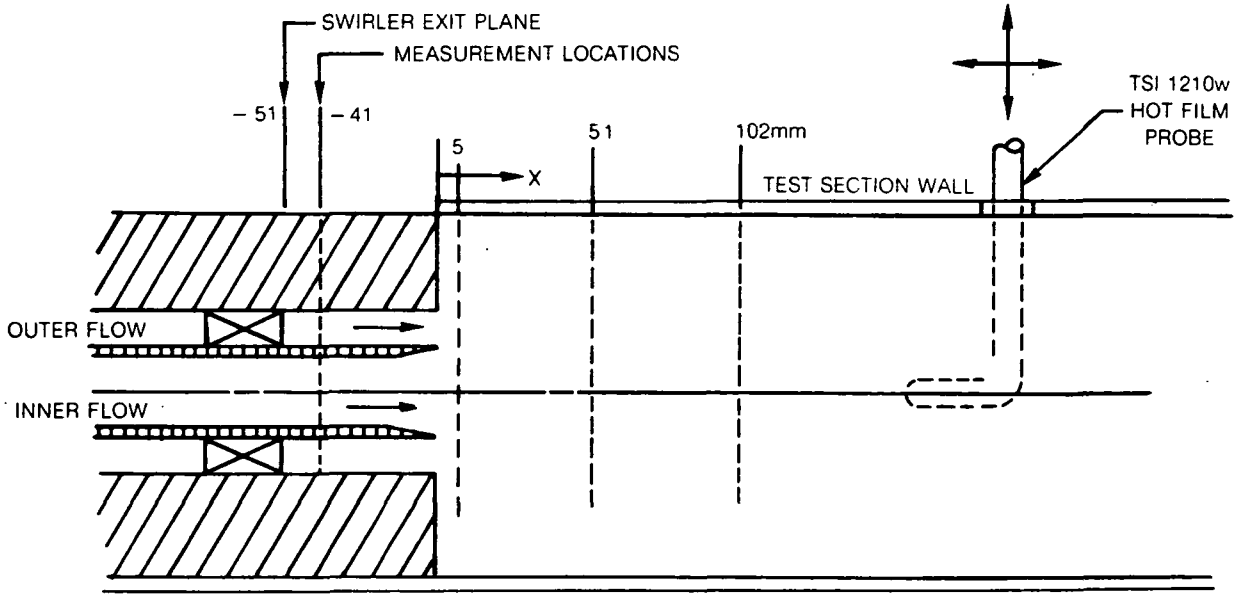

MEAN AXIAL VELOCITY PROFILES FOR NONSWIRLING FLOW WITH TAPERED INNER JET INLET

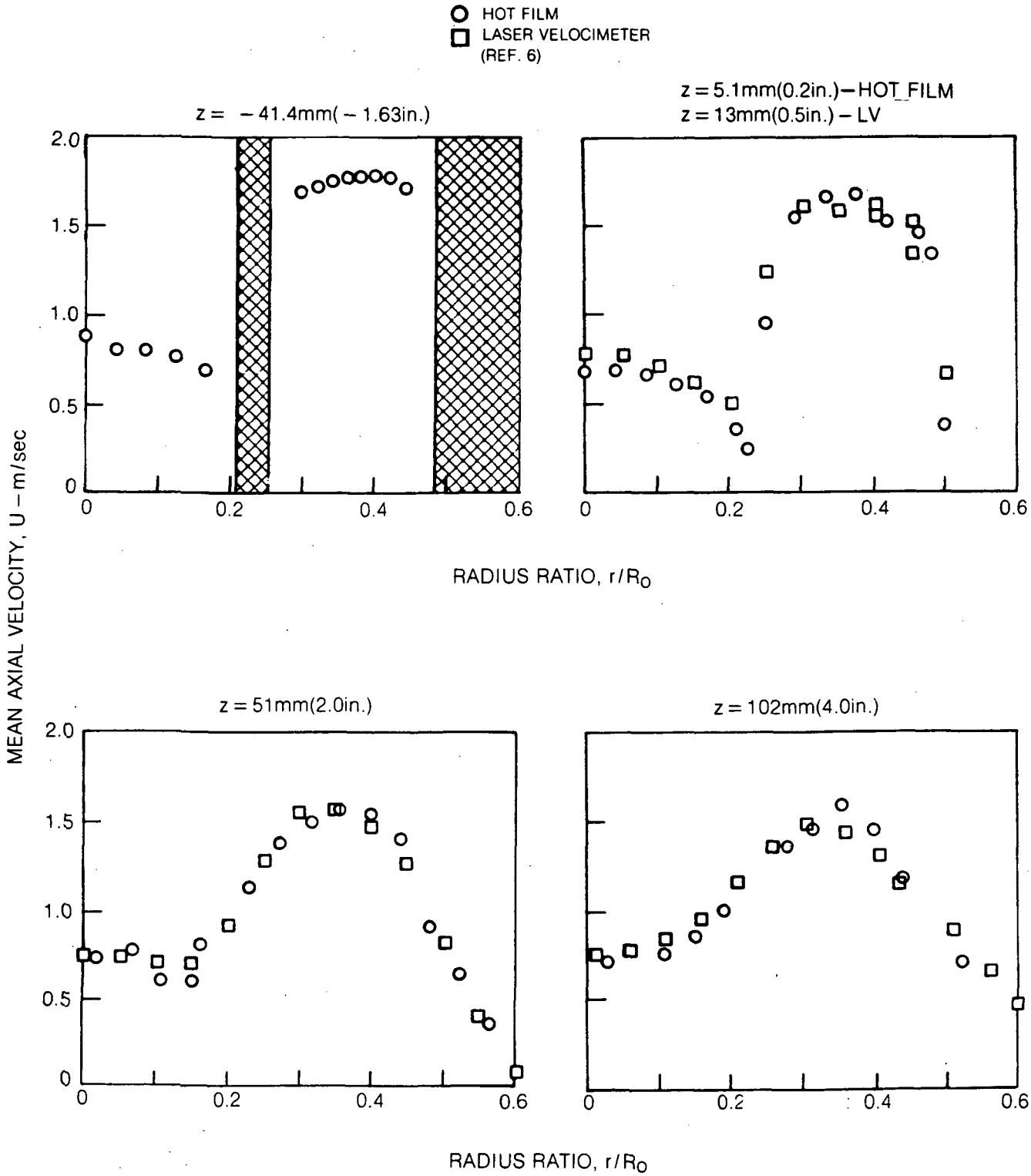

84-9-1-3

FLUCTUATING AXIAL VELOCITY PROFILES FOR NONSWIRLING FLOW WITH TAPERED INNER JET INLET

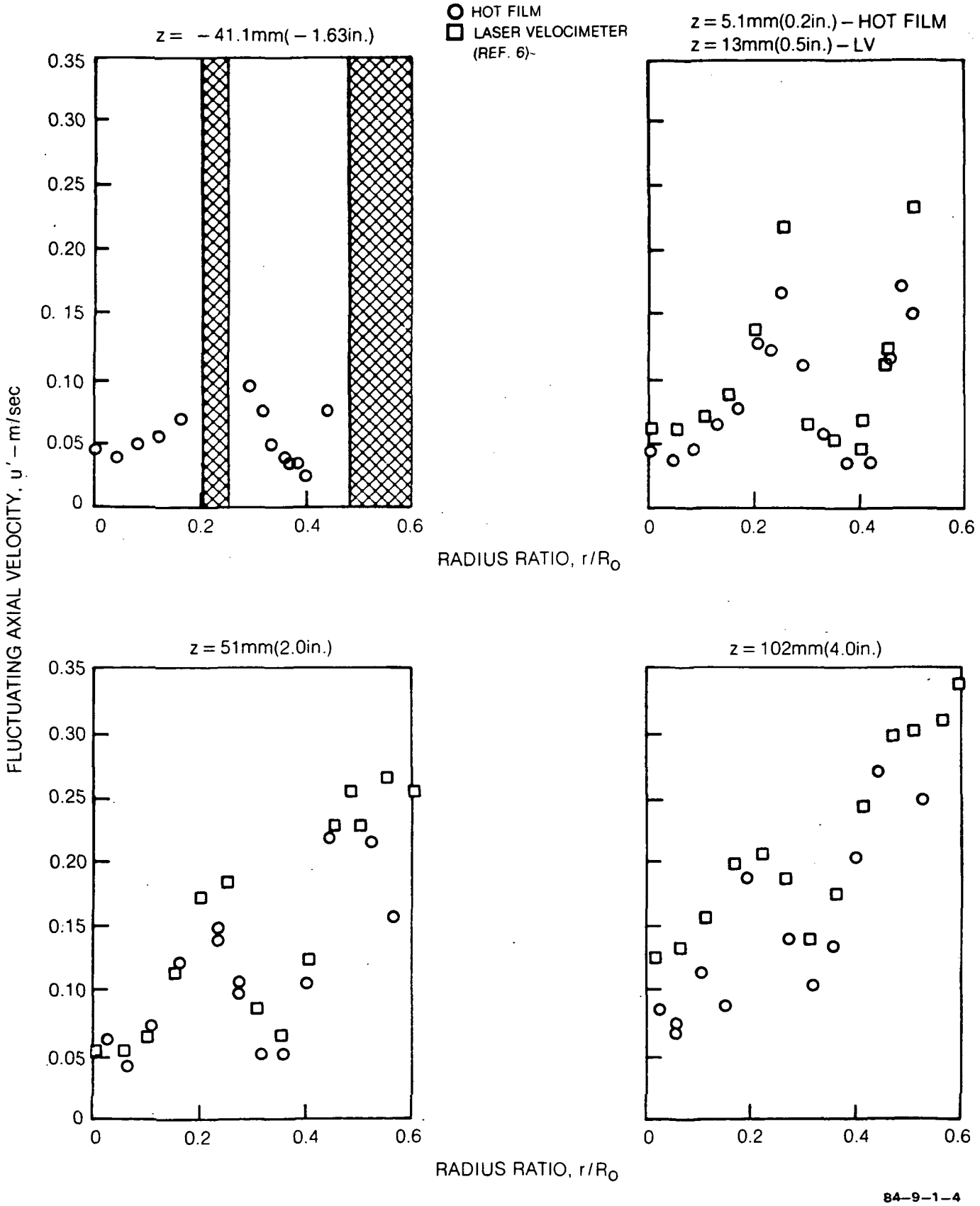

84-9-1-4

DISSIPATION RATE FOR NONSWIRLING FLOW WITH TAPERED INNER JET INLET

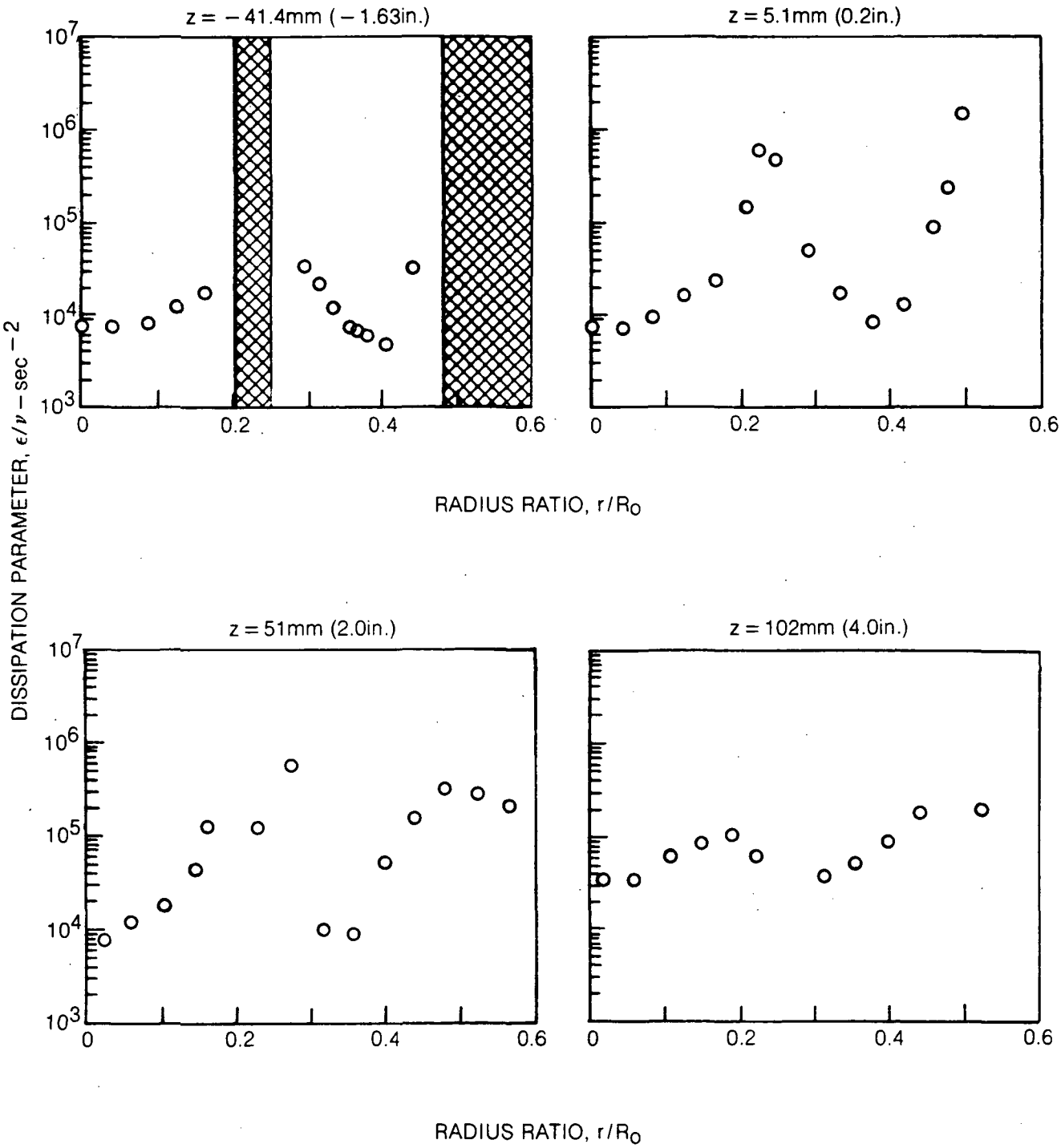

84-9-1-5

LENGTH SCALE DISTRIBUTION FOR NONSWIRLING FLOW WITH TAPERED INNER JET INLET

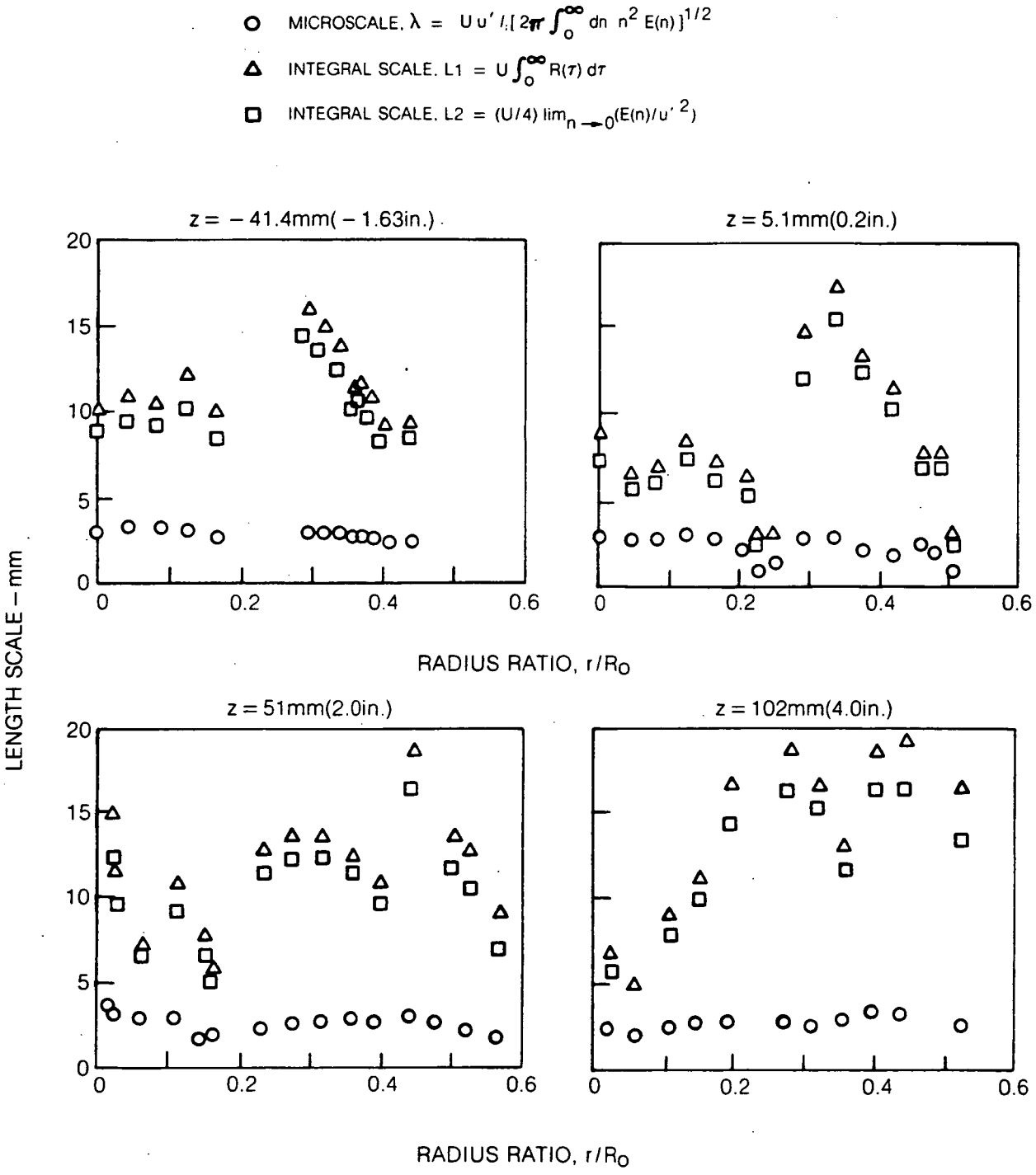

84-9-1-6

MEAN AND FLUCTUATING AXIAL VELOCITY PROFILES FOR SWIRLING FLOW WITH TAPERED INNER JET INLET

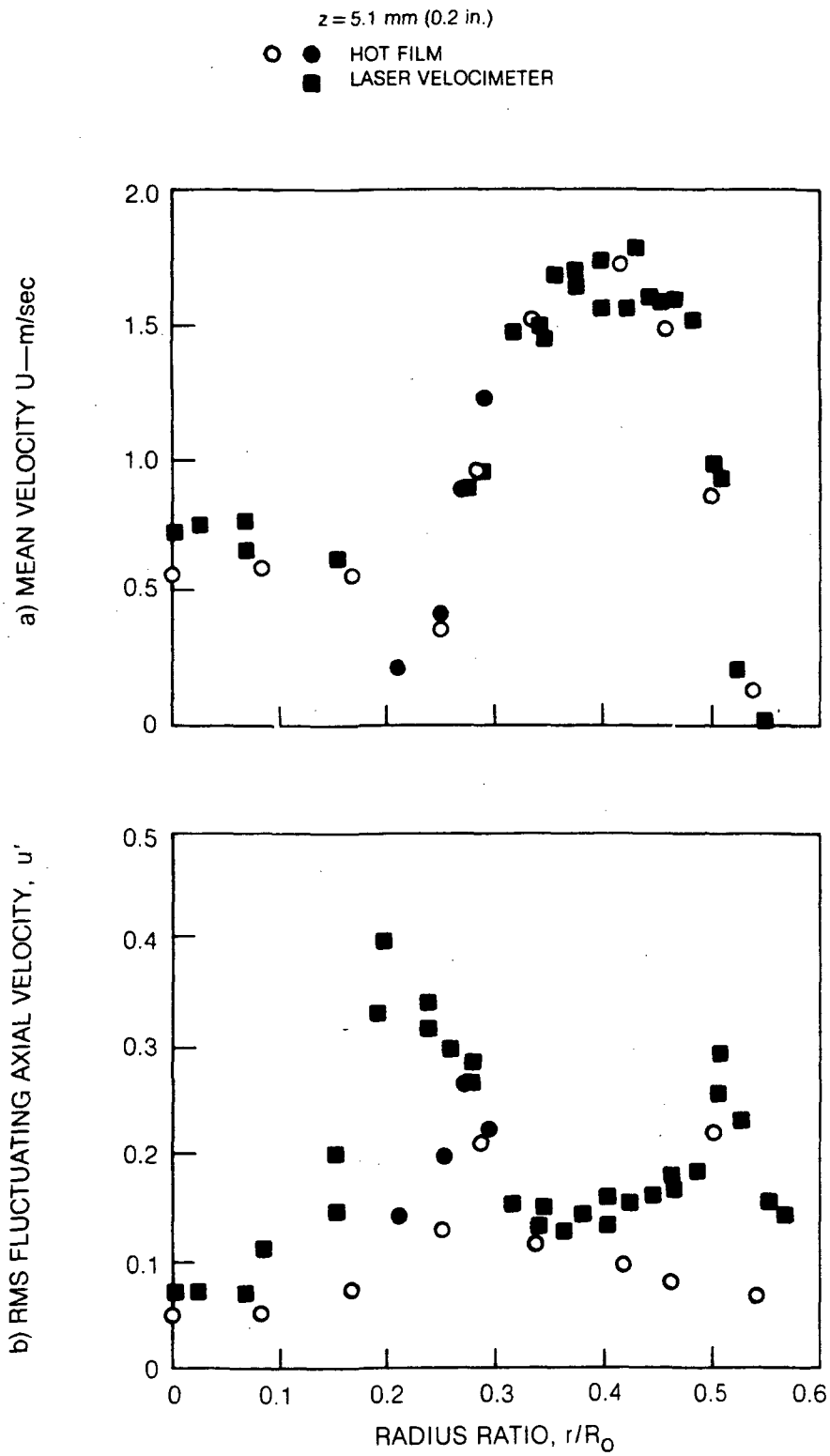

85-6-9-5

DISSIPATION RATE AND LENGTH SCALES DISTRIBUTION FOR SWIRLING FLOW WITH TAPERED INNER JET INLET

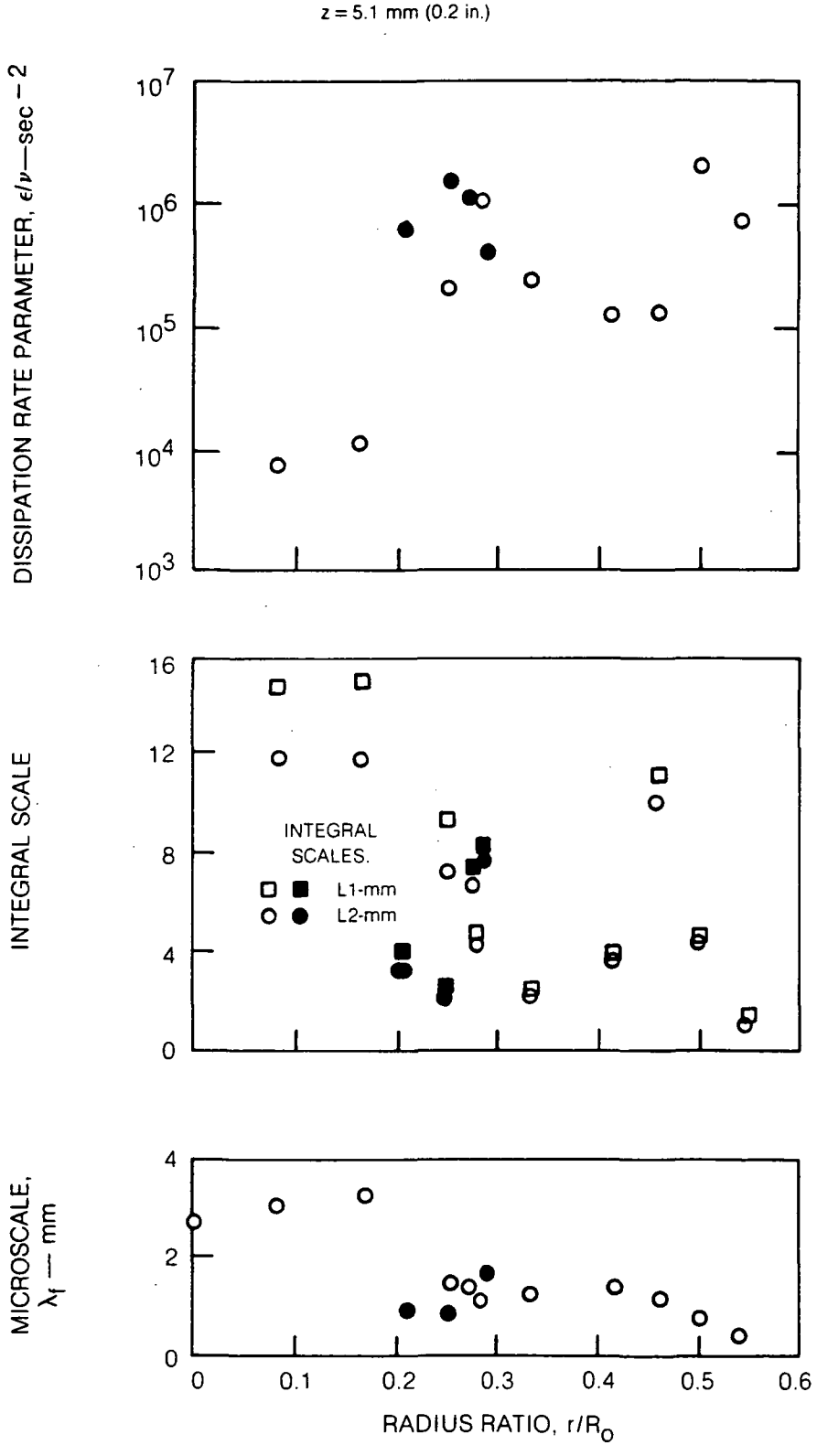

85-6-9-6

FIG. 10

OPTICAL ARRANGEMENT FOR TWO COMPONENT LV MEASUREMENTS

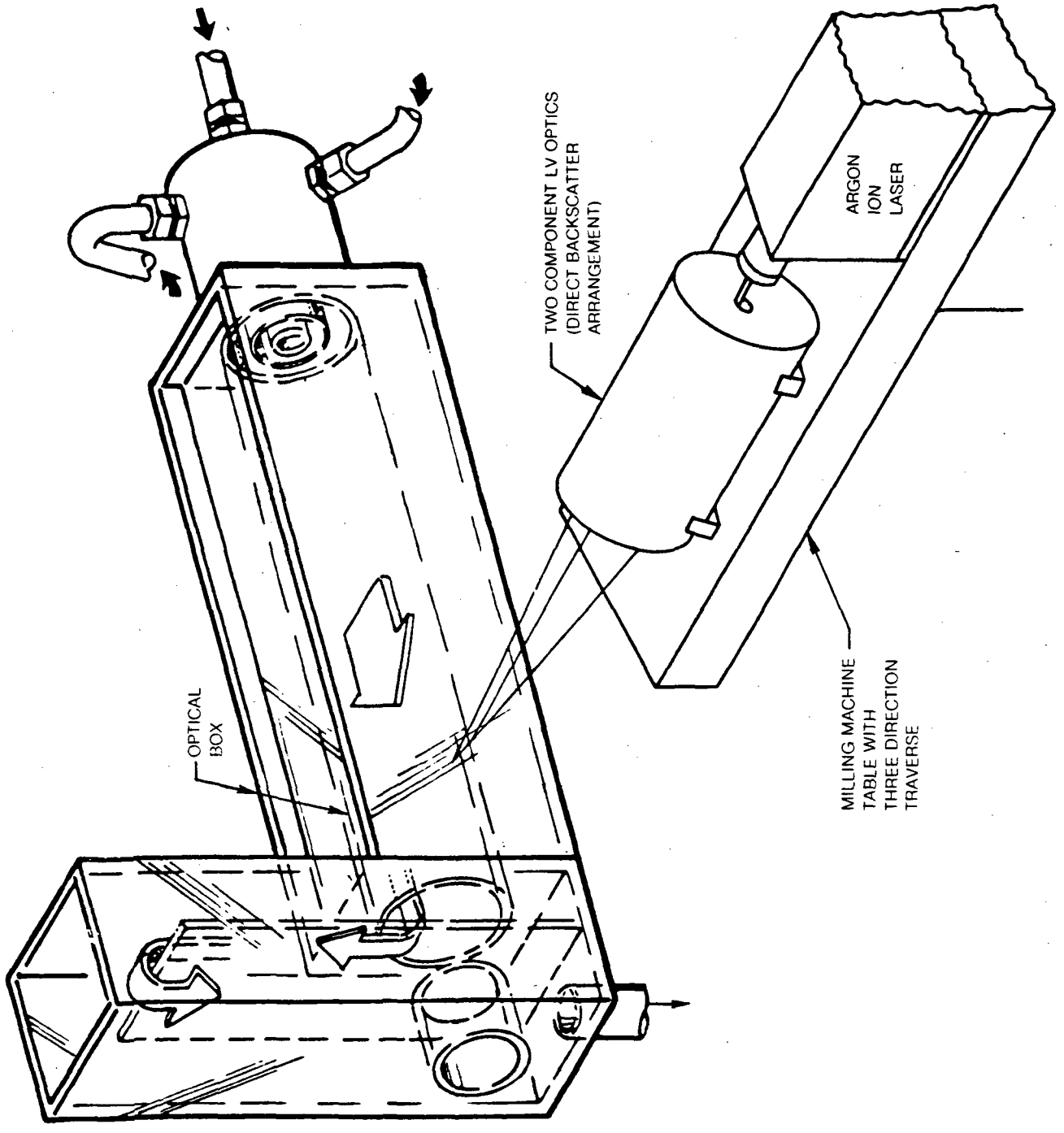

81-12-38-7

SKETCH OF OPTICAL COMPONENTS AND BEAM PATHS USED FOR TWO COMPONENT VELOCITY MEASUREMENTS

OPTICAL COMPONENTS

02 — BACKCOVER PLATE WITH POLARIZATION ROTATOR
03 — BEAM SPLITTER SECTION 1
04 — BRAGG CELL SECTIONS
05 — BEAM SPLITTER SECTION 2
06 — BACKSCATTER SECTION WITH GREEN LASER LINE FILTER
07 — BACKSCATTER SECTION WITH BLUE LASER LINE FILTER
08 — PHOTOMULTIPLIER TUBE
09 — LENS MOUNT
10 — PINHOLE SECTION
11 — BEAM TRANSLATOR
12 — BEAM EXPANDER

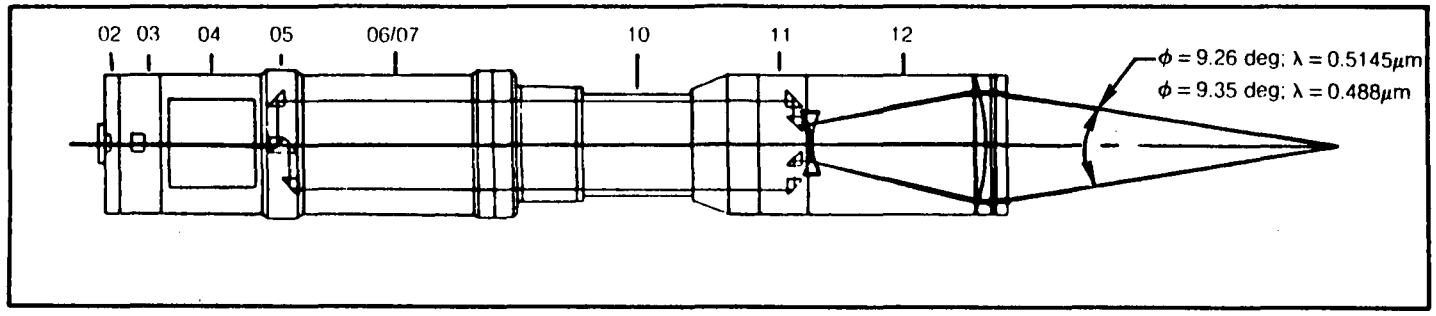

TRANSMITTER BEAM PATH

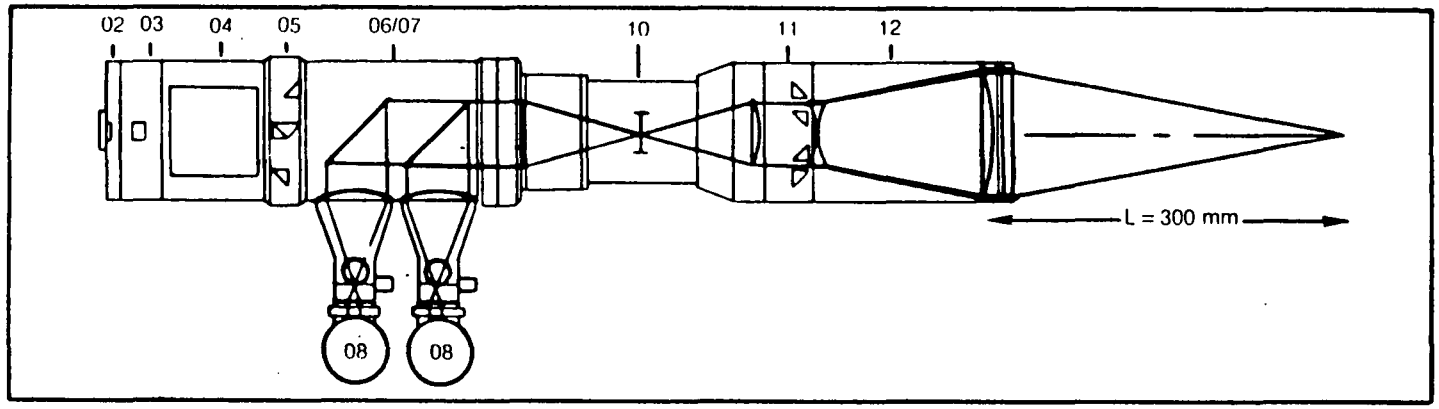

RECEIVER BEAM PATH

FIG. 12

MEAN AXIAL VELOCITY PROFILES

SYMBOL	○	●	□	■
LOCATION, θ	0	180	90	270
RUN NOS.	6, 9, 10, 11		7	

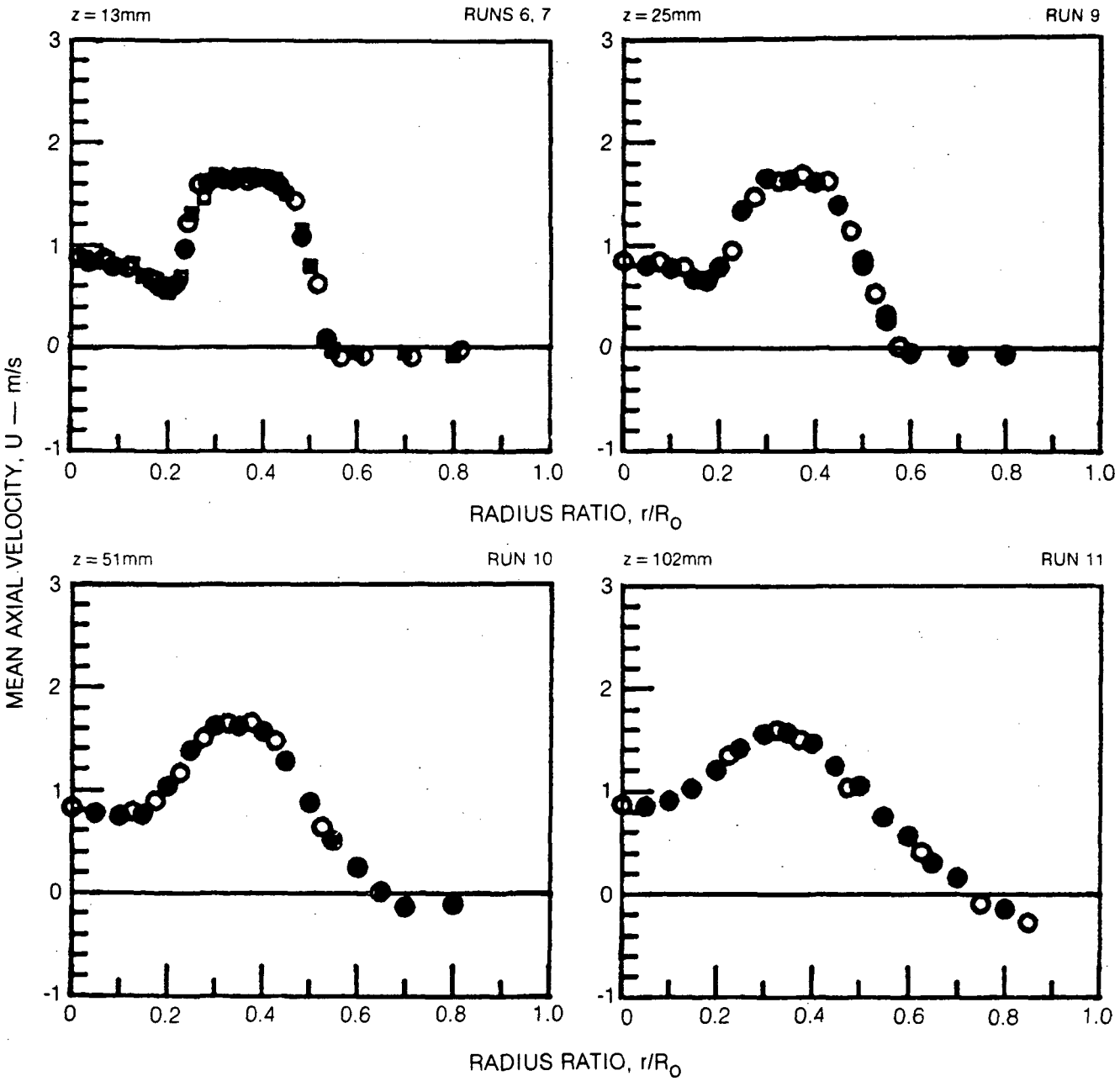

84-5-29-1

MEAN AXIAL VELOCITY PROFILES (CONT.)

SYMBOL	○	●
LOCATION, θ	0	180

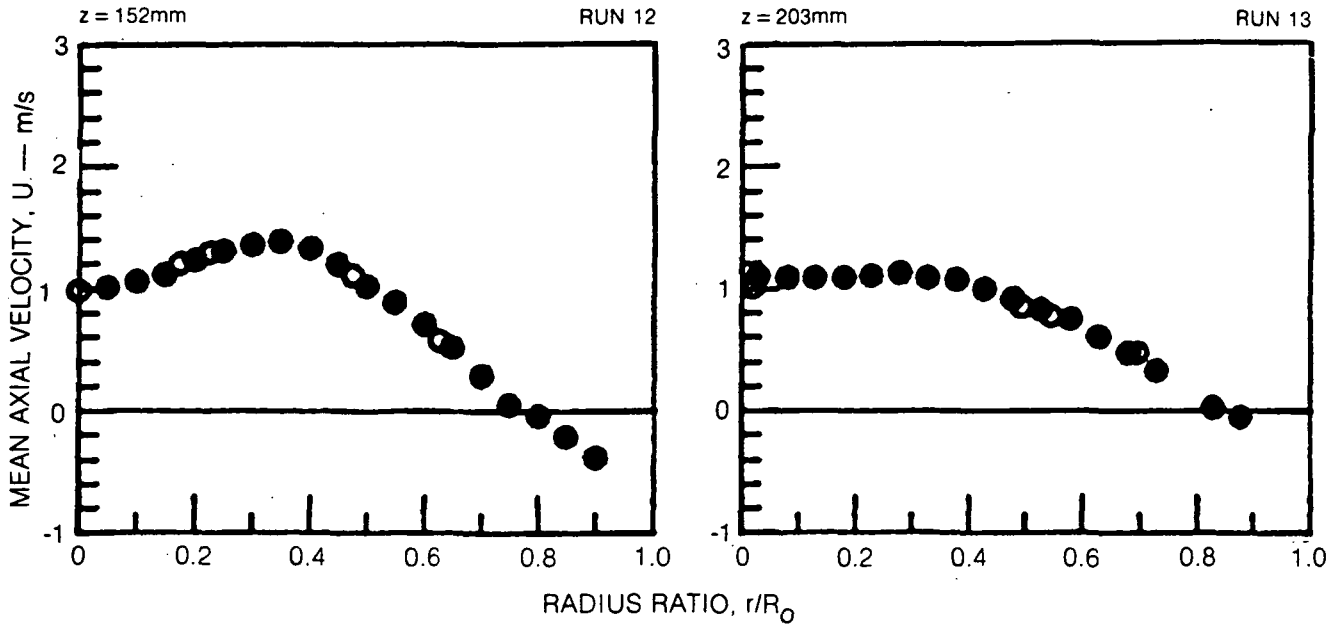

FIG. 13

MEAN RADIAL VELOCITY PROFILES

SYMBOL	○	●
LOCATION, θ	0	180

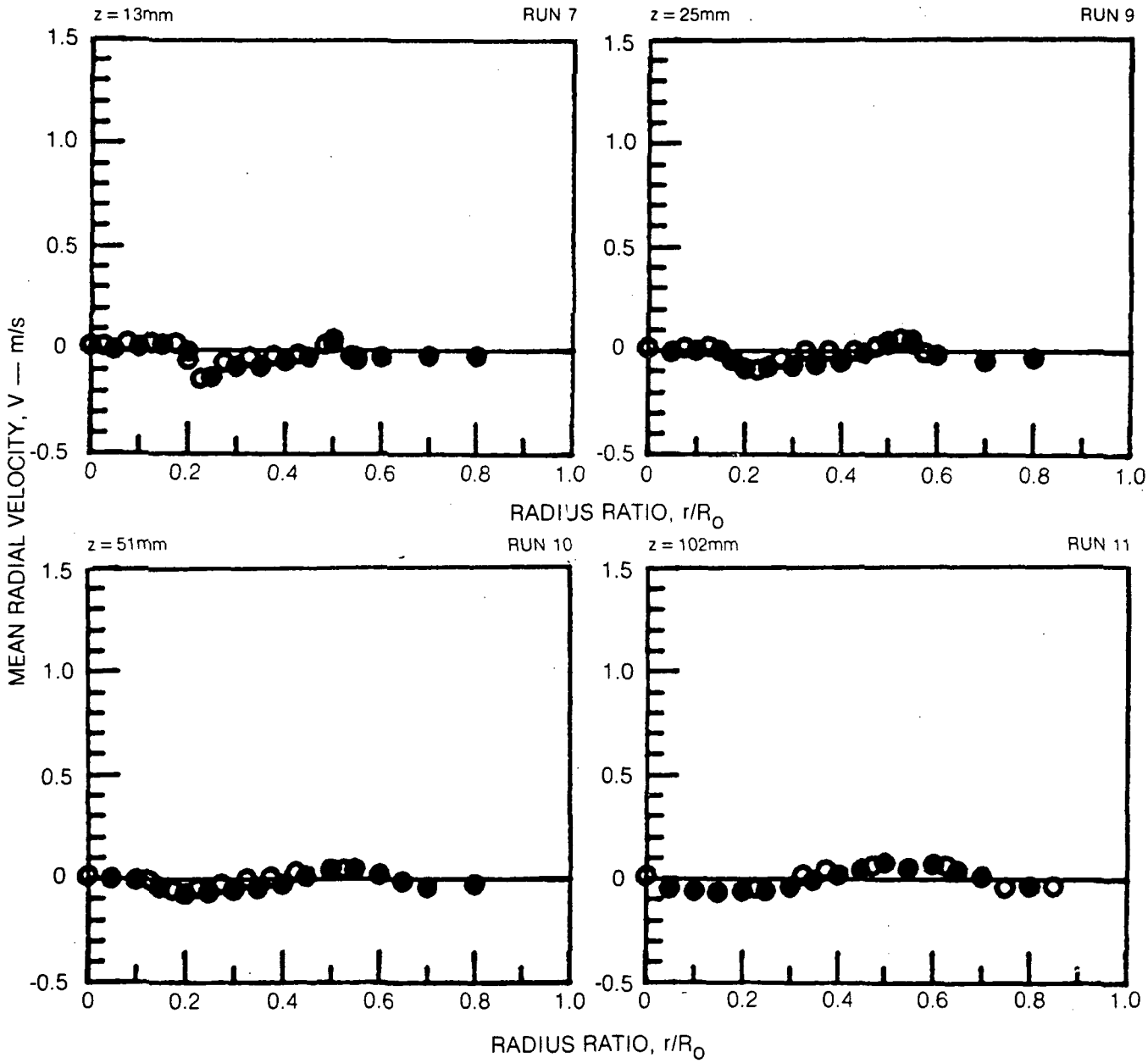

84–5–29–3

MEAN RADIAL VELOCITY PROFILES (CONT.)

SYMBOL	○	●
LOCATION, θ	0	180

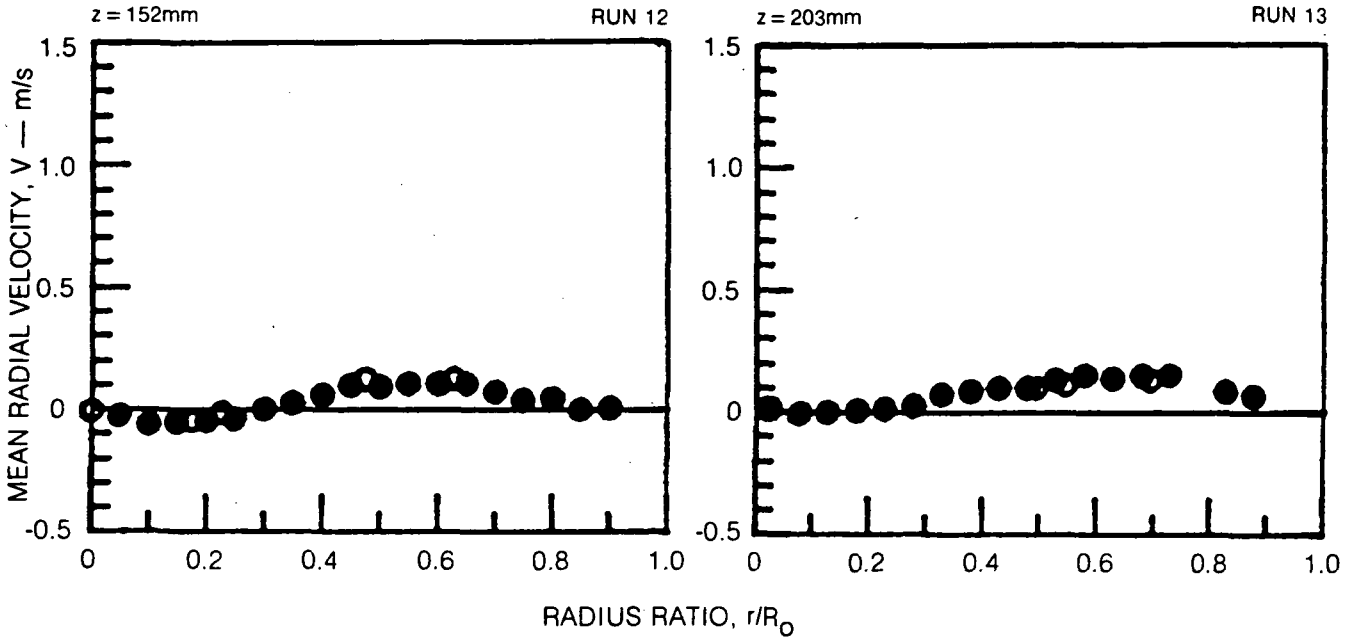

FLUCTUATING AXIAL VELOCITY PROFILES

SYMBOL	○	●	□	■
LOCATION, θ	0	180	270	90
RUN NOS.	6, 9, 10, 11		7	

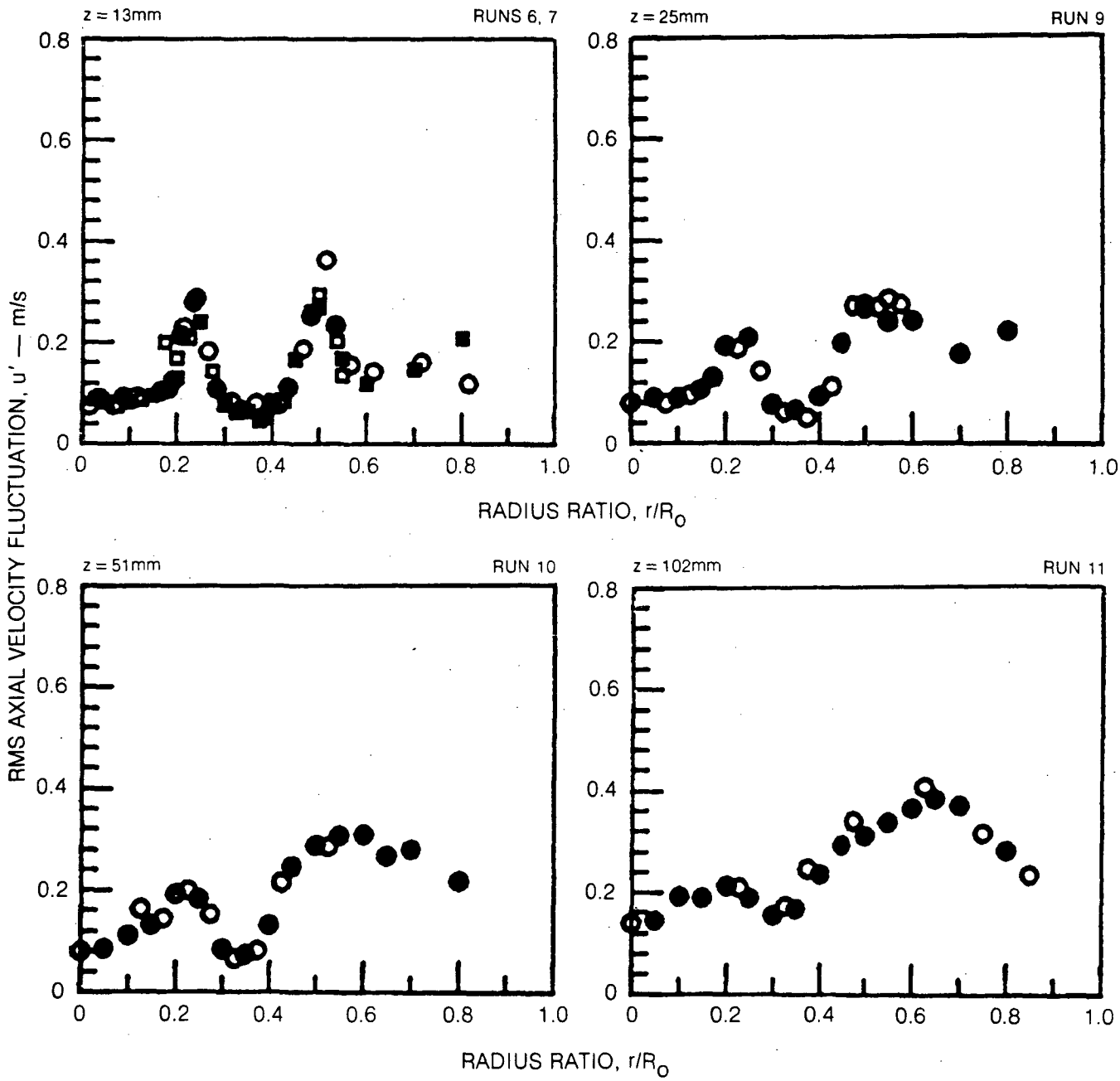

84-5-29-5

FLUCTUATING AXIAL VELOCITY PROFILES (CONT.)

SYMBOL	○	●
LOCATION, θ	0	180

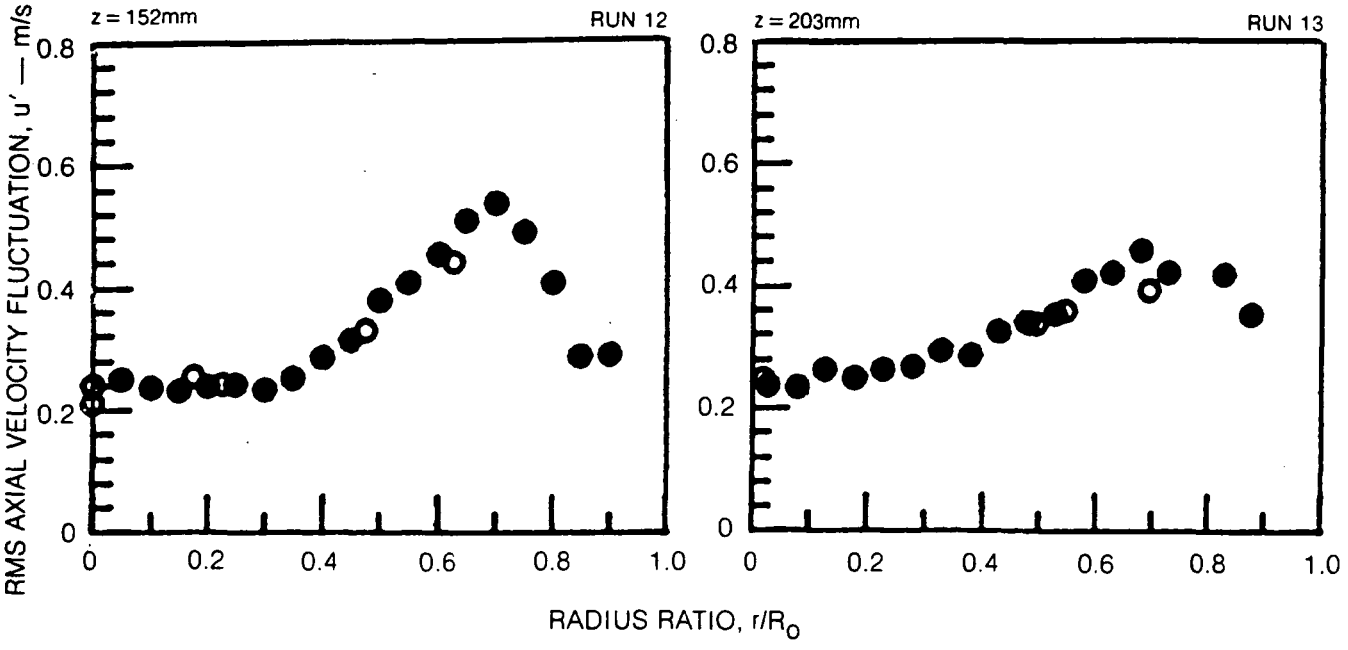

FLUCTUATING RADIAL VELOCITY PROFILES

SYMBOL	○	●
LOCATION, θ	0	180

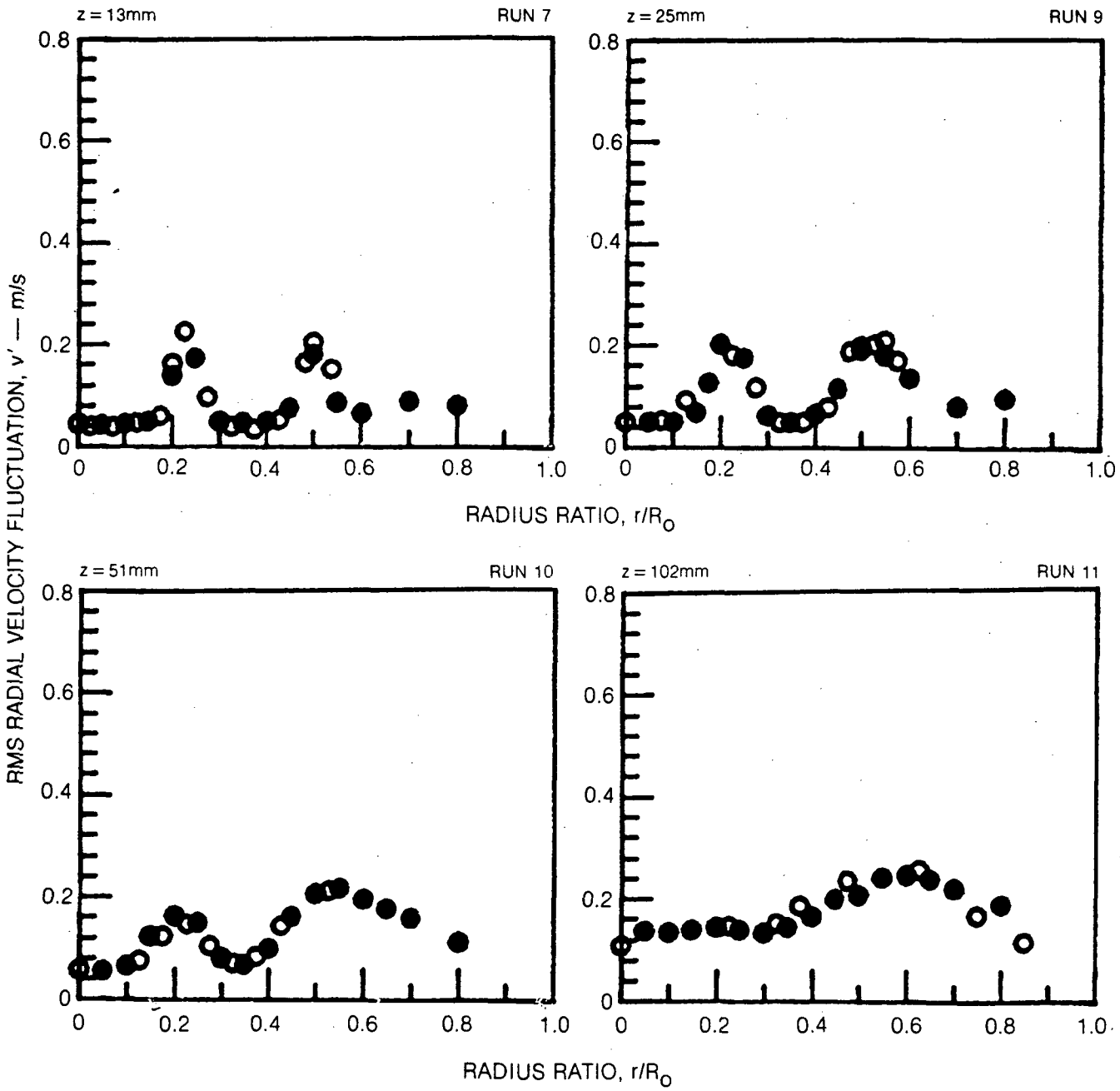

84–5–29–7

FLUCTUATING RADIAL VELOCITY PROFILES (CONT.)

SYMBOL	○	●
LOCATION, θ	0	180

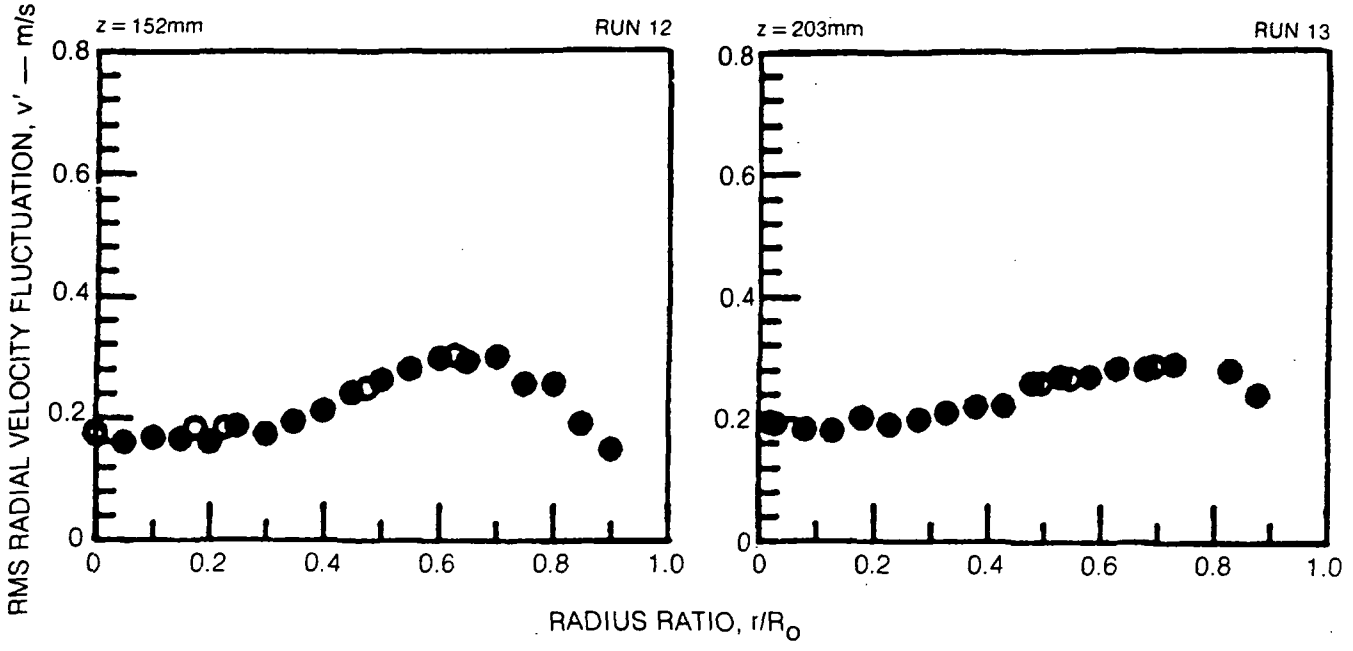

FIG. 16

MOMENTUM TRANSPORT RATE, $\overline{uv}$, PROFILES

SYMBOL	○	●
LOCATION, θ	0	180

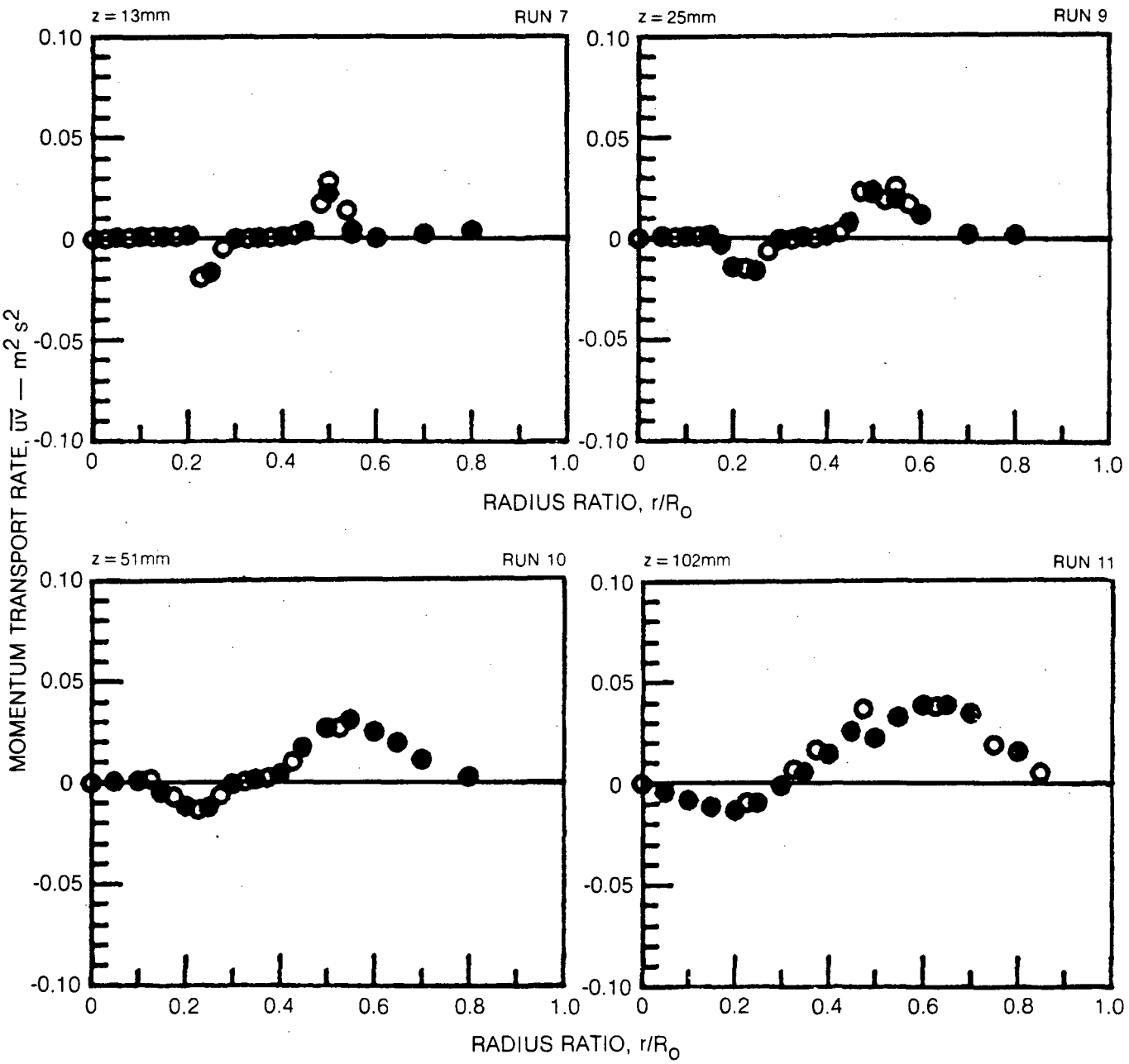

84-5-29-9

FIG. 16 (CONT)

MOMENTUM TRANSPORT RATE, $\overline{uv}$, PROFILES (CONT.)

SYMBOL	O	●
LOCATION, θ	0	180

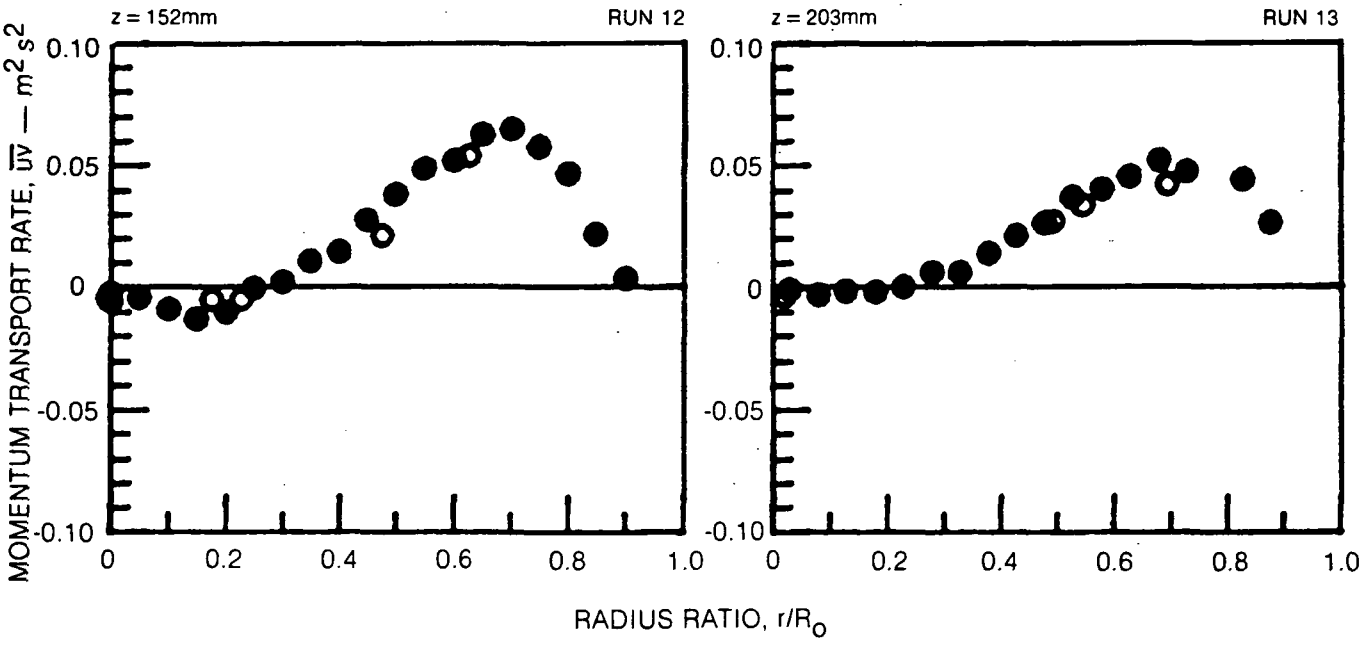

FIG. 17

MOMENTUM TRANSPORT CORRELATION COEFFICIENT, R_{uv}, PROFILES

SYMBOL	○	●
LOCATION, θ	0	180

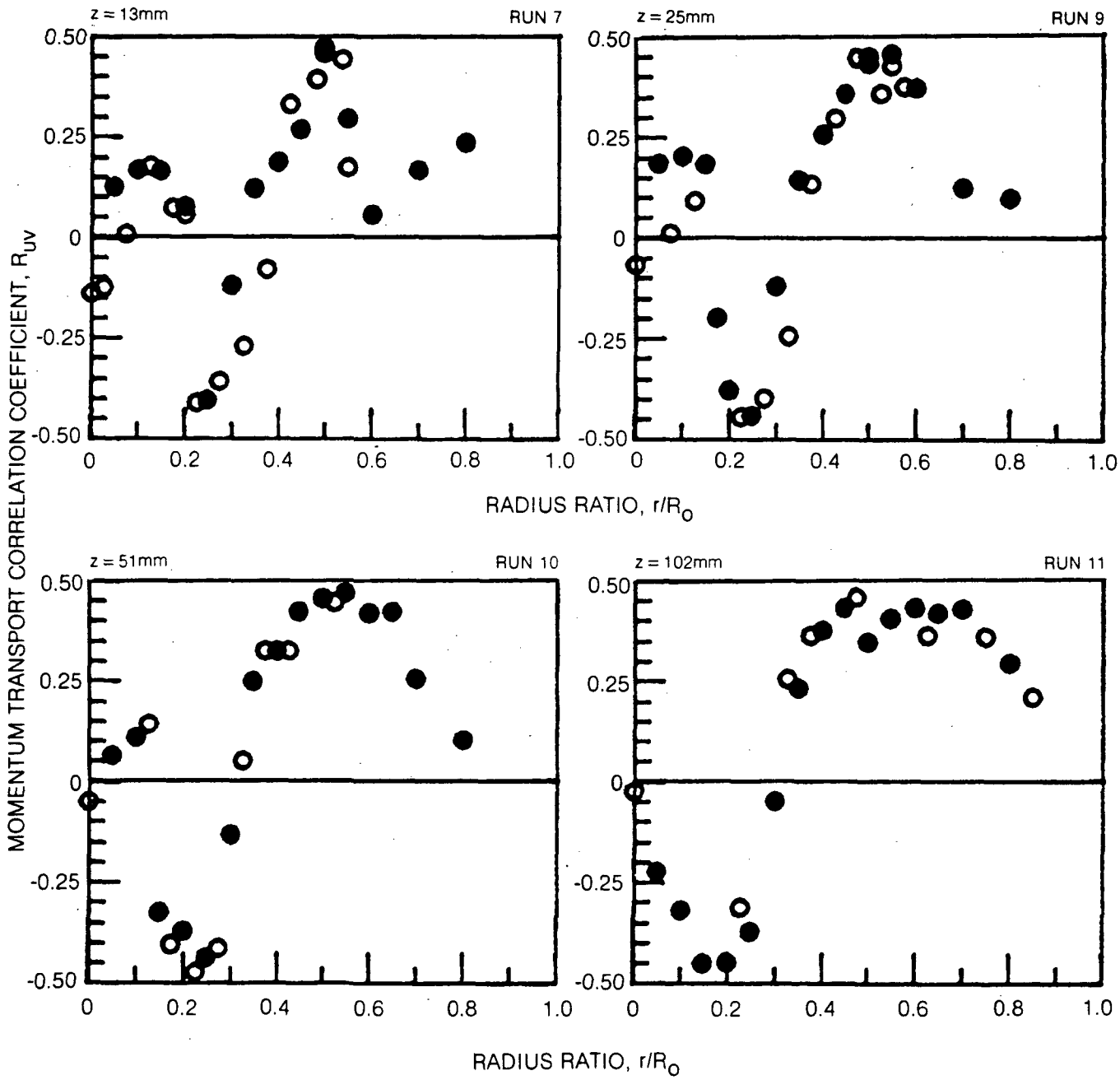

84-5-29-11

MOMENTUM TRANSPORT CORRELATION COEFFICIENT, R_{uv}, PROFILES (CONT.)

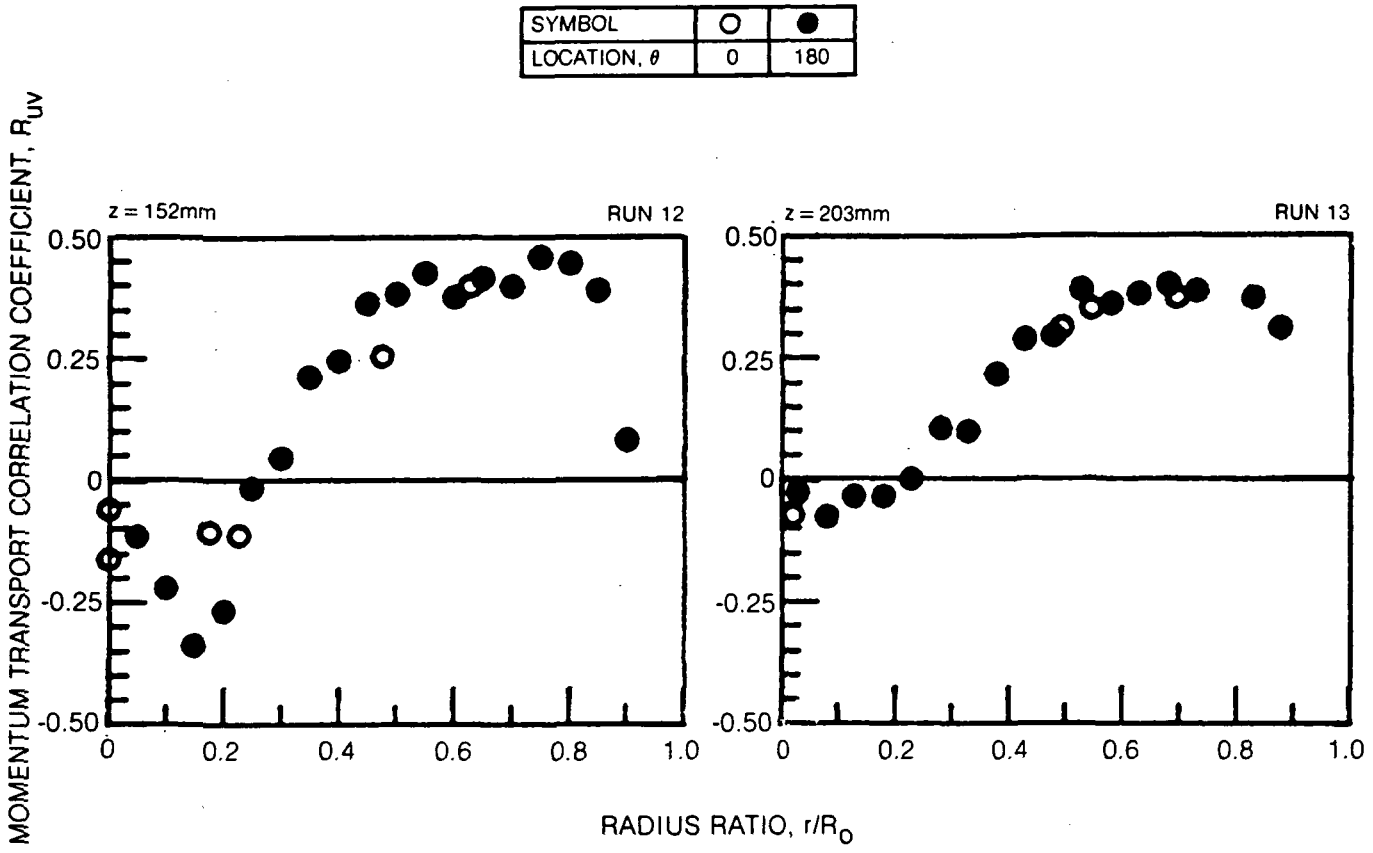

MEAN INNER JET FLUID CONCENTRATION PROFILES

	HORIZONTAL TRAVERSE	VERTICAL TRAVERSE
OPEN SYMBOLS:	$\theta = 90°$	$\theta = 0°$
SOLID SYMBOLS:	$\theta = 270°$	$\theta = 180°$

SYMBOL	○	●	⊡	■
RUN NOS.	24, 18, 19, 20		25, 26, 27	

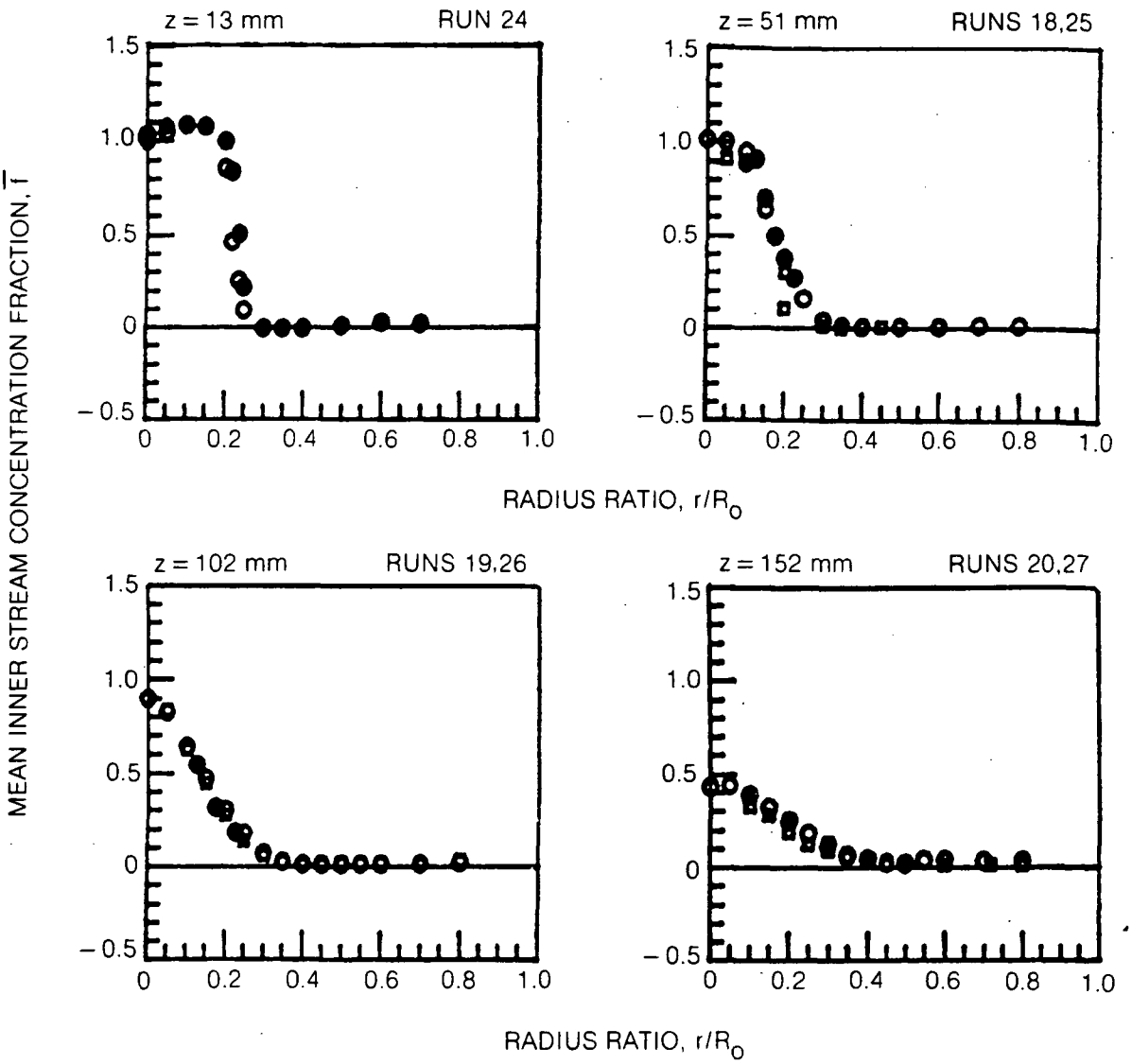

MEAN INNER JET FLUID CONCENTRATION PROFILES (CONT.)

	HORIZONTAL TRAVERSE	VERTICAL TRAVERSE
OPEN SYMBOLS:	$\theta = 90°$	$\theta = 0°$
SOLID SYMBOLS:	$\theta = 270°$	$\theta = 180°$

SYMBOL	○	●	□	■
RUN NOS.	21		28	

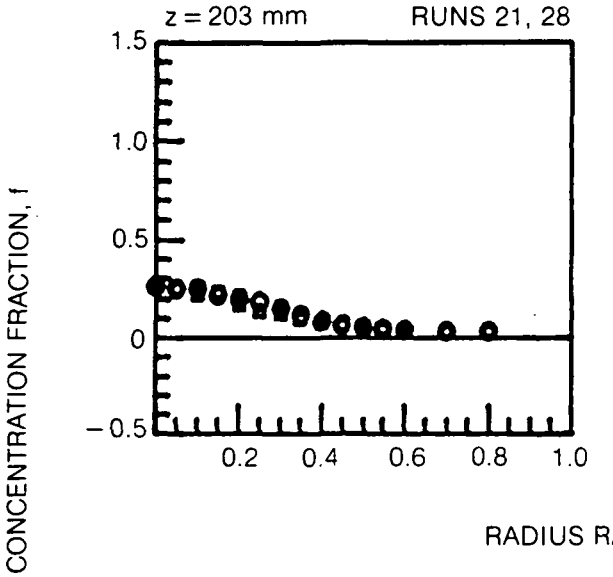

FLUCTUATING INNER JET FLUID CONCENTRATION PROFILES

	HORIZONTAL TRAVERSE	VERTICAL TRAVERSE
OPEN SYMBOLS SOLID SYMBOLS	$\theta = 90°$ $\theta = 270°$	$\theta = 0°$ $\theta = 180°$

SYMBOL	○	●	□	■
RUN NOS	24. 18. 19. 20		25. 26. 27	

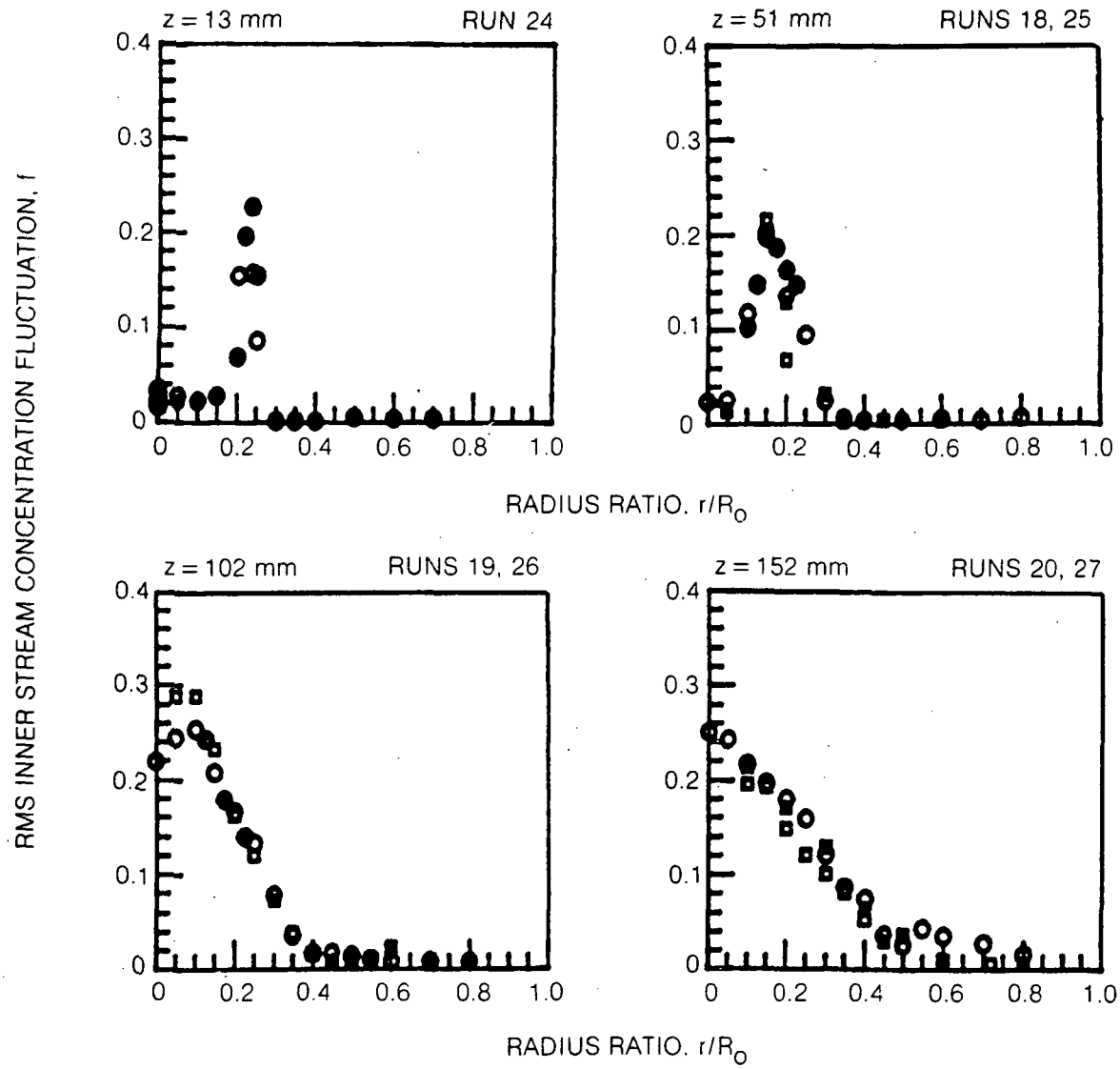

85-6-9-3

FIG. 19 (CONT)

FLUCTUATING INNER JET FLUID CONCENTRATION PROFILES (CONT.)

	HORIZONTAL TRAVERSE	VERTICAL TRAVERSE
OPEN SYMBOLS:	$\theta = 90°$	$\theta = 0°$
SOLID SYMBOLS:	$\theta = 270°$	$\theta = 180°$

SYMBOL	○	●	⊡	■
RUN NOS	21		28	

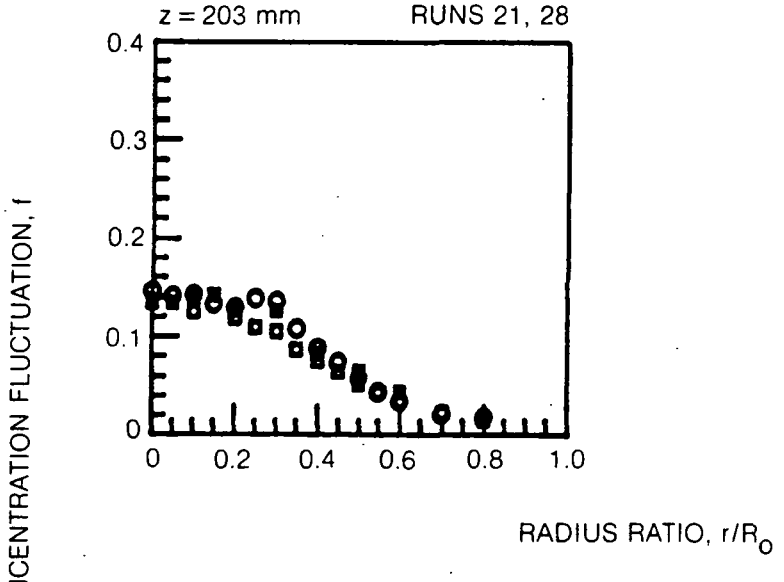

1. Report No.	2. Government Accession No.	3. Recipient's Catalog No.
NASA CR-174831		

4. Title and Subtitle	5. Report Date
Turbulent Transport and Length Scale Measurement Experiments with Conbined Coaxial Jets	November, 1984
	6. Performing Organization Code

7. Author(s)	8. Performing Organization Report No.
Bruce V. Johnson Richard Roback	R84-915540-34
	10. Work Unit No.

9. Performing Organization Name and Address	11. Contract or Grant No.
United Technologies Research Center Silver Lane East Hartford, CT 06108	NAS3-2271
	13. Type of Report and Period Covered Interium Report 9/1/83-8/16/84

12. Sponsoring Agency Name and Address	14. Sponsoring Agency Code
NASA Lewis Research Center 21000 Brookpark Road Cleveland, OH 44135	

15. Supplementary Notes

Project Manager, Cecil J. Marek, NASA LeRC

16. Abstract

A three phase experimental study of mixing downstream of swirling and nonswirling confined coaxial jets was conducted to obtain data for the evaluation and improvement of turbulent transport models currently employed in a variety of computational procedures used throughout the propulsion community. The present effort (Phase III) was directed toward (1) the acquisition of length scale and dissipation rate data that provide more accurate inlet boundary conditions for the computational procedures and a data base to evaluate the turbulent transport models in the near jet region where recirculation does not occur, and (2) the acquisition of mass and momentum turbulent transport data for a nonswirling flow condition with a blunt inner-jet inlet configuration rather than the tapered inner-jet inlet employed in Phase I. A measurement technique, generally used to obtain approximate integral length and microscales of turbulence and dissipation rates, was computerized. This computerized procedure was used to obtain at the test conditions where mass and momentum turbulent transport data had been previously obtained in Phases I and II. Results showed the dissipation rate varied by 2 1/2 orders of magnitude across the inlet plane, by 2 orders of magnitude 51 mm from the inlet plane, and by 1 order of magnitude at 102 mm from the inlet plane for a nonswirling flow test conditions.

17. Key Words (Suggested by Author(s))	18. Distribution Statement
Experiment, Coaxial Jets, Turbulant Transport, Length Scale, Dissipation Rate, Spectrum Measurements	Unclassified - Unlimited

19. Security Classif. (of this report)	20. Security Classif. (of this page)	21. No. of pages	22. Price*
Unclassified	Unclassified		

*For sale by the National Technical Information Service, Springfield, Virginia 22161